Ambiguity-Free Measurement of cos 2β: Time-Integrated and Time-Dependent Angular Analyses of $B \rightarrow J/\psi K\pi$

The *BABAR* Collaboration

B. Aubert, R. Barate, D. Boutigny, F. Couderc, J.-M. Gaillard,
Y. Karyotakis, J. P. Lees, V. Poireau, V. Tisserand, and A. Zghiche
Laboratoire de Physique des Particules, F-74941 Annecy-le-Vieux, France

A. Palano and A. Pompili
Università di Bari, Dipartimento di Fisica and INFN, I-70126 Bari, Italy

J. C. Chen, N. D. Qi, G. Rong, P. Wang, and Y. S. Zhu
Institute of High Energy Physics, Beijing 100039, China

G. Eigen, I. Ofte, and B. Stugu
University of Bergen, Inst. of Physics, N-5007 Bergen, Norway

G. S. Abrams, A. W. Borgland, A. B. Breon, D. N. Brown, J. Button-Shafer, R. N. Cahn,
E. Charles, C. T. Day, M. S. Gill, A. V. Gritsan, Y. Groysman, R. G. Jacobsen, R. W. Kadel,
J. Kadyk, L. T. Kerth, Yu. G. Kolomensky, G. Kukartsev, G. Lynch, L. M. Mir, P. J. Oddone,
T. J. Orimoto, M. Pripstein, N. A. Roe, M. T. Ronan, V. G. Shelkov, and W. A. Wenzel
Lawrence Berkeley National Laboratory and University of California, Berkeley, CA 94720, USA

M. Barrett, K. E. Ford, T. J. Harrison, A. J. Hart, C. M. Hawkes, S. E. Morgan, and A. T. Watson
University of Birmingham, Birmingham, B15 2TT, United Kingdom

M. Fritsch, K. Goetzen, T. Held, H. Koch, B. Lewandowski, M. Pelizaeus, and M. Steinke
Ruhr Universität Bochum, Institut für Experimentalphysik 1, D-44780 Bochum, Germany

J. T. Boyd, N. Chevalier, W. N. Cottingham, M. P. Kelly, T. E. Latham, and F. F. Wilson
University of Bristol, Bristol BS8 1TL, United Kingdom

T. Cuhadar-Donszelmann, C. Hearty, N. S. Knecht, T. S. Mattison, J. A. McKenna, and D. Thiessen
University of British Columbia, Vancouver, BC, Canada V6T 1Z1

A. Khan, P. Kyberd, and L. Teodorescu
Brunel University, Uxbridge, Middlesex UB8 3PH, United Kingdom

A. E. Blinov, V. E. Blinov, V. P. Druzhinin, V. B. Golubev, V. N. Ivanchenko, E. A. Kravchenko,
A. P. Onuchin, S. I. Serednyakov, Yu. I. Skovpen, E. P. Solodov, and A. N. Yushkov
Budker Institute of Nuclear Physics, Novosibirsk 630090, Russia

D. Best, M. Bruinsma, M. Chao, I. Eschrich, D. Kirkby, A. J. Lankford,
M. Mandelkern, R. K. Mommsen, W. Roethel, and D. P. Stoker
University of California at Irvine, Irvine, CA 92697, USA

C. Buchanan and B. L. Hartfiel

University of California at Los Angeles, Los Angeles, CA 90024, USA

S. D. Foulkes, J. W. Gary, B. C. Shen, and K. Wang

University of California at Riverside, Riverside, CA 92521, USA

D. del Re, H. K. Hadavand, E. J. Hill, D. B. MacFarlane, H. P. Paar, Sh. Rahatlou, and V. Sharma

University of California at San Diego, La Jolla, CA 92093, USA

J. Adam Cunha, J. W. Berryhill, C. Campagnari, B. Dahmes, T. M. Hong,
O. Long, A. Lu, M. A. Mazur, J. D. Richman, and W. Verkerke

University of California at Santa Barbara, Santa Barbara, CA 93106, USA

T. W. Beck, A. M. Eisner, C. A. Heusch, J. Kroseberg, W. S. Lockman, G. Nesom,
T. Schalk, B. A. Schumm, A. Seiden, P. Spradlin, D. C. Williams, and M. G. Wilson

University of California at Santa Cruz, Institute for Particle Physics, Santa Cruz, CA 95064, USA

J. Albert, E. Chen, G. P. Dubois-Felsmann, A. Dvoretskii, D. G. Hitlin,
I. Narsky, T. Piatenko, F. C. Porter, A. Ryd, A. Samuel, and S. Yang

California Institute of Technology, Pasadena, CA 91125, USA

S. Jayatilleke, G. Mancinelli, B. T. Meadows, and M. D. Sokoloff

University of Cincinnati, Cincinnati, OH 45221, USA

F. Blanc, P. Bloom, S. Chen, W. T. Ford, U. Nauenberg, A. Olivas, P. Rankin, J. G. Smith, J. Zhang, and L. Zhang

University of Colorado, Boulder, CO 80309, USA

A. Chen, J. L. Harton, A. Soffer, W. H. Toki, R. J. Wilson, and Q. Zeng

Colorado State University, Fort Collins, CO 80523, USA

D. Altenburg, T. Brandt, J. Brose, M. Dickopp, E. Feltresi, A. Hauke, H. M. Lacker, R. Müller-Pfefferkorn,
R. Nogowski, S. Otto, A. Petzold, J. Schubert, K. R. Schubert, R. Schwierz, B. Spaan, and J. E. Sundermann

Technische Universität Dresden, Institut für Kern- und Teilchenphysik, D-01062 Dresden, Germany

D. Bernard, G. R. Bonneaud, F. Brochard, P. Grenier, S. Schrenk, Ch. Thiebaux, G. Vasileiadis, and M. Verderi

Ecole Polytechnique, LLR, F-91128 Palaiseau, France

D. J. Bard, P. J. Clark, D. Lavin, F. Muheim, S. Playfer, and Y. Xie

University of Edinburgh, Edinburgh EH9 3JZ, United Kingdom

M. Andreotti, V. Azzolini, D. Bettoni, C. Bozzi, R. Calabrese,
G. Cibinetto, E. Luppi, M. Negrini, L. Piemontese, and A. Sarti

Università di Ferrara, Dipartimento di Fisica and INFN, I-44100 Ferrara, Italy

E. Treadwell

Florida A&M University, Tallahassee, FL 32307, USA

F. Anulli, R. Baldini-Ferroli, A. Calcaterra, R. de Sangro,
G. Finocchiaro, P. Patteri, I. M. Peruzzi, M. Piccolo, and A. Zallo

Laboratori Nazionali di Frascati dell'INFN, I-00044 Frascati, Italy

A. Buzzo, R. Capra, R. Contri, G. Crosetti, M. Lo Vetere, M. Macri,
M. R. Monge, S. Passaggio, C. Patrignani, E. Robutti, A. Santroni, and S. Tosi

Università di Genova, Dipartimento di Fisica and INFN, I-16146 Genova, Italy

S. Bailey, G. Brandenburg, K. S. Chaisanguanthum, M. Morii, and E. Won

Harvard University, Cambridge, MA 02138, USA

R. S. Dubitzky, U. Langenegger, J. Marks, and U. Uwer
Universität Heidelberg, Physikalisches Institut, Philosophenweg 12, D-69120 Heidelberg, Germany

W. Bhimji, D. A. Bowerman, P. D. Dauncey, U. Egede, J. R. Gaillard,
G. W. Morton, J. A. Nash, M. B. Nikolich, and G. P. Taylor
Imperial College London, London, SW7 2AZ, United Kingdom

M. J. Charles, G. J. Grenier, and U. Mallik
University of Iowa, Iowa City, IA 52242, USA

J. Cochran, H. B. Crawley, J. Lamsa, W. T. Meyer, S. Prell, E. I. Rosenberg, A. E. Rubin, and J. Yi
Iowa State University, Ames, IA 50011-3160, USA

M. Biasini, R. Covarelli, and M. Pioppi
Università di Perugia, Dipartimento di Fisica and INFN, I-06100 Perugia, Italy

M. Davier, X. Giroux, G. Grosdidier, A. Höcker, S. Laplace, F. Le Diberder, V. Lepeltier,
A. M. Lutz, T. C. Petersen, S. Plaszczynski, M. H. Schune, L. Tantot, and G. Wormser
Laboratoire de l'Accélérateur Linéaire, F-91898 Orsay, France

C. H. Cheng, D. J. Lange, M. C. Simani, and D. M. Wright
Lawrence Livermore National Laboratory, Livermore, CA 94550, USA

A. J. Bevan, C. A. Chavez, J. P. Coleman, I. J. Forster, J. R. Fry, E. Gabathuler,
R. Gamet, D. E. Hutchcroft, R. J. Parry, D. J. Payne, R. J. Sloane, and C. Touramanis
University of Liverpool, Liverpool L69 7ZE, United Kingdom

C. M. Cormack and F. Di Lodovico
Queen Mary, University of London, E1 4NS, United Kingdom

C. L. Brown, G. Cowan, R. L. Flack, H. U. Flaecher, M. G. Green,
P. S. Jackson, T. R. McMahon, S. Ricciardi, F. Salvatore, and M. A. Winter
University of London, Royal Holloway and Bedford New College, Egham, Surrey TW20 0EX, United Kingdom

D. Brown and C. L. Davis
University of Louisville, Louisville, KY 40292, USA

J. Allison, N. R. Barlow, R. J. Barlow, M. C. Hodgkinson, G. D. Lafferty, A. J. Lyon, and J. C. Williams
University of Manchester, Manchester M13 9PL, United Kingdom

A. Farbin, W. D. Hulsbergen, A. Jawahery, D. Kovalskyi, C. K. Lae, V. Lillard, and D. A. Roberts
University of Maryland, College Park, MD 20742, USA

G. Blaylock, C. Dallapiccola, S. S. Hertzbach, R. Kofler,
V. B. Koptchev, T. B. Moore, S. Saremi, H. Staengle, and S. Willocq
University of Massachusetts, Amherst, MA 01003, USA

R. Cowan, G. Sciolla, S. J. Sekula, F. Taylor, and R. K. Yamamoto
Massachusetts Institute of Technology, Laboratory for Nuclear Science, Cambridge, MA 02139, USA

D. J. J. Mangeol, P. M. Patel, and S. H. Robertson
McGill University, Montréal, QC, Canada H3A 2T8

A. Lazzaro, V. Lombardo, and F. Palombo
Università di Milano, Dipartimento di Fisica and INFN, I-20133 Milano, Italy

J. M. Bauer, L. Cremaldi, V. Eschenburg, R. Godang, R. Kroeger,
J. Reidy, D. A. Sanders, D. J. Summers, and H. W. Zhao

University of Mississippi, University, MS 38677, USA

S. Brunet, D. Côté, and P. Taras
Université de Montréal, Laboratoire René J. A. Lévesque, Montréal, QC, Canada H3C 3J7

H. Nicholson
Mount Holyoke College, South Hadley, MA 01075, USA

N. Cavallo,* F. Fabozzi,* C. Gatto, L. Lista, D. Monorchio, P. Paolucci, D. Piccolo, and C. Sciacca
Università di Napoli Federico II, Dipartimento di Scienze Fisiche and INFN, I-80126, Napoli, Italy

M. Baak, H. Bulten, G. Raven, H. L. Snoek, and L. Wilden
NIKHEF, National Institute for Nuclear Physics and High Energy Physics, NL-1009 DB Amsterdam, The Netherlands

C. P. Jessop and J. M. LoSecco
University of Notre Dame, Notre Dame, IN 46556, USA

T. Allmendinger, K. K. Gan, K. Honscheid, D. Hufnagel, H. Kagan,
R. Kass, T. Pulliam, A. M. Rahimi, R. Ter-Antonyan, and Q. K. Wong
Ohio State University, Columbus, OH 43210, USA

J. Brau, R. Frey, O. Igonkina, C. T. Potter, N. B. Sinev, D. Strom, and E. Torrence
University of Oregon, Eugene, OR 97403, USA

F. Colecchia, A. Dorigo, F. Galeazzi, M. Margoni, M. Morandin,
M. Posocco, M. Rotondo, F. Simonetto, R. Stroili, G. Tiozzo, and C. Voci
Università di Padova, Dipartimento di Fisica and INFN, I-35131 Padova, Italy

M. Benayoun, H. Briand, J. Chauveau, P. David, Ch. de la Vaissière, L. Del Buono, O. Hamon,
M. J. J. John, Ph. Leruste, J. Malcles, J. Ocariz, M. Pivk, L. Roos, S. T'Jampens, and G. Therin
Universités Paris VI et VII, Laboratoire de Physique Nucléaire et de Hautes Energies, F-75252 Paris, France

P. F. Manfredi and V. Re
Università di Pavia, Dipartimento di Elettronica and INFN, I-27100 Pavia, Italy

P. K. Behera, L. Gladney, Q. H. Guo, and J. Panetta
University of Pennsylvania, Philadelphia, PA 19104, USA

C. Angelini, G. Batignani, S. Bettarini, M. Bondioli, F. Bucci, G. Calderini,
M. Carpinelli, F. Forti, M. A. Giorgi, A. Lusiani, G. Marchiori, F. Martinez-Vidal,†
M. Morganti, N. Neri, E. Paoloni, M. Rama, G. Rizzo, F. Sandrelli, and J. Walsh
Università di Pisa, Dipartimento di Fisica, Scuola Normale Superiore and INFN, I-56127 Pisa, Italy

M. Haire, D. Judd, K. Paick, and D. E. Wagoner
Prairie View A&M University, Prairie View, TX 77446, USA

N. Danielson, P. Elmer, Y. P. Lau, C. Lu, V. Miftakov, J. Olsen, A. J. S. Smith, and A. V. Telnov
Princeton University, Princeton, NJ 08544, USA

F. Bellini, R. Faccini, F. Ferrarotto, F. Ferroni, M. Gaspero, L. Li Gioi,
M. A. Mazzoni, S. Morganti, M. Pierini, G. Piredda, F. Safai Tehrani, and C. Voena
Università di Roma La Sapienza, Dipartimento di Fisica and INFN, I-00185 Roma, Italy

G. Cavoto
Princeton University, Princeton, NJ 08544, USA and
Università di Roma La Sapienza, Dipartimento di Fisica and INFN, I-00185 Roma, Italy

S. Christ, G. Wagner, and R. Waldi

Universität Rostock, D-18051 Rostock, Germany

T. Adye, N. De Groot, B. Franek, N. I. Geddes, G. P. Gopal, and E. O. Olaiya
Rutherford Appleton Laboratory, Chilton, Didcot, Oxon, OX11 0QX, United Kingdom

R. Aleksan, S. Emery, A. Gaidot, S. F. Ganzhur, P.-F. Giraud, G. Hamel de Monchenault,
W. Kozanecki, M. Legendre, G. W. London, B. Mayer, G. Schott, G. Vasseur, Ch. Yèche, and M. Zito
DSM/Dapnia, CEA/Saclay, F-91191 Gif-sur-Yvette, France

M. V. Purohit, A. W. Weidemann, J. R. Wilson, and F. X. Yumiceva
University of South Carolina, Columbia, SC 29208, USA

T. Abe, D. Aston, R. Bartoldus, N. Berger, A. M. Boyarski, O. L. Buchmueller, R. Claus,
M. R. Convery, M. Cristinziani, G. De Nardo, D. Dong, J. Dorfan, D. Dujmic, W. Dunwoodie,
E. E. Elsen, S. Fan, R. C. Field, T. Glanzman, S. J. Gowdy, T. Hadig, V. Halyo, C. Hast, T. Hryn'ova,
W. R. Innes, M. H. Kelsey, P. Kim, M. L. Kocian, D. W. G. S. Leith, J. Libby, S. Luitz, V. Luth,
H. L. Lynch, H. Marsiske, R. Messner, D. R. Muller, C. P. O'Grady, V. E. Ozcan, A. Perazzo,
M. Perl, S. Petrak, B. N. Ratcliff, A. Roodman, A. A. Salnikov, R. H. Schindler, J. Schwiening,
G. Simi, A. Snyder, A. Soha, J. Stelzer, D. Su, M. K. Sullivan, J. Va'vra, S. R. Wagner, M. Weaver,
A. J. R. Weinstein, W. J. Wisniewski, M. Wittgen, D. H. Wright, A. K. Yarritu, and C. C. Young
Stanford Linear Accelerator Center, Stanford, CA 94309, USA

P. R. Burchat, A. J. Edwards, T. I. Meyer, B. A. Petersen, and C. Roat
Stanford University, Stanford, CA 94305-4060, USA

M. Ahmed, S. Ahmed, M. S. Alam, J. A. Ernst, M. A. Saeed, M. Saleem, and F. R. Wappler
State University of New York, Albany, NY 12222, USA

W. Bugg, M. Krishnamurthy, and S. M. Spanier
University of Tennessee, Knoxville, TN 37996, USA

R. Eckmann, H. Kim, J. L. Ritchie, A. Satpathy, and R. F. Schwitters
University of Texas at Austin, Austin, TX 78712, USA

J. M. Izen, I. Kitayama, X. C. Lou, and S. Ye
University of Texas at Dallas, Richardson, TX 75083, USA

F. Bianchi, M. Bona, F. Gallo, and D. Gamba
Università di Torino, Dipartimento di Fisica Sperimentale and INFN, I-10125 Torino, Italy

L. Bosisio, C. Cartaro, F. Cossutti, G. Della Ricca, S. Dittongo,
S. Grancagnolo, L. Lanceri, P. Poropat,[‡] L. Vitale, and G. Vuagnin
Università di Trieste, Dipartimento di Fisica and INFN, I-34127 Trieste, Italy

R. S. Panvini
Vanderbilt University, Nashville, TN 37235, USA

Sw. Banerjee, C. M. Brown, D. Fortin, P. D. Jackson, R. Kowalewski, J. M. Roney, and R. J. Sobie
University of Victoria, Victoria, BC, Canada V8W 3P6

J. J. Back, P. F. Harrison, and G. B. Mohanty
Department of Physics, University of Warwick, Coventry CV4 7AL, United Kingdom

H. R. Band, X. Chen, B. Cheng, S. Dasu, M. Datta, A. M. Eichenbaum, K. T. Flood,
M. Graham, J. J. Hollar, J. R. Johnson, P. E. Kutter, H. Li, R. Liu, A. Mihalyi, Y. Pan,
R. Prepost, P. Tan, J. H. von Wimmersperg-Toeller, J. Wu, S. L. Wu, and Z. Yu
University of Wisconsin, Madison, WI 53706, USA

M. G. Greene and H. Neal

Yale University, New Haven, CT 06511, USA

(Dated: November 2, 2004)

We present results on $B \to J/\psi K\pi$ decays using e^+e^- annihilation data collected with the *BABAR* detector at the $\Upsilon(4S)$ resonance. The detector is located at the PEP-II asymmetric-energy storage ring facility at the Stanford Linear Accelerator Center. Using approximately 88 million $B\overline{B}$ pairs, we measure the decay amplitudes for the flavor eigenmodes and observe strong-phase differences indicative of final-state interactions with a significance of 7.6 standard deviations. We use the interference between the $K\pi$ S-wave and P-wave amplitudes in the region of the $K^*(892)$ to resolve the ambiguity in the determination of these strong phases. We then perform an ambiguity-free measurement of $\cos 2\beta$ using the angular and time-dependent asymmetry in $B \to J/\psi K^{*0}(K_S^0\pi^0)$ decays. With $\sin 2\beta$ fixed at its measured value and $\cos 2\beta$ treated as an independent parameter, we find $\cos 2\beta = 2.72^{+0.50}_{-0.79}(\text{stat}) \pm 0.27(\text{syst})$, determining the sign of $\cos 2\beta$ to be positive at 86% CL.

PACS numbers: 13.25.Hw, 12.15.Hh, 14.40.Nd, 11.30.Er

The Standard Model of electroweak interactions describes *CP* violation in weak interactions of quarks by the presence of a nonzero phase in the three-generation Cabibbo-Kobayashi-Maskawa (CKM) quark-mixing matrix [1]. In this framework, the *CP*-violation parameter $\sin 2\beta$ can be measured by examining the proper-time distributions of neutral B-meson decays to final states containing a charmonium meson and a neutral kaon. The Belle [2] and *BABAR* [3] experiments have recently performed precise measurements of $\sin 2\beta$, leading to a world average of 0.731 ± 0.056 [4]. These measurements determine β up to a four-fold ambiguity, corresponding to the two different signs of $\cos 2\beta$ and the transformation $\beta \to \pi + \beta$.

One of the possible values of β is compatible with measurements of other quantities that constrain the Unitarity Triangle [4]. However, it is still possible that, because of contributions from new physics, the actual value of β is one of the three other values consistent with the measurement of $\sin 2\beta$ [5–7]. A measurement of the sign of $\cos 2\beta$ would either agree with the standard interpretation $\beta \approx 0.41$ and with its indistinguishable nonstandard alternative $\beta \approx 0.41 + \pi$, or would exclude these and instead imply the nonstandard solutions $\beta \approx 1.16$ and $\beta \approx 1.16 + \pi$.

Several strategies to determine $\cos 2\beta$ have been proposed [6], [8–13]. In particular, $\cos 2\beta$ appears as a factor in the interference between the *CP*-odd and the two *CP*-even amplitudes in the time- and angle-dependent distribution describing the decay $B \to J/\psi K^{*0}$ ($K^{*0} \to K_S^0\pi^0$, $J/\psi \to \ell^+\ell^-$) [14–17]. However, neither this distribution nor the time-integrated angular distributions of the companion channels $B^0 \to J/\psi K^{*0}(K^{*0} \to K^+\pi^-)$ and $B^+ \to J/\psi K^{*+}$ (and related charge-conjugate decays) can resolve a two-fold ambiguity in the relative strong phases among the three $B \to J/\psi K^*$ decay amplitudes.

This leaves an overall sign ambiguity in $\cos 2\beta$ [18, 19]. Resolving the ambiguity from these partial waves alone would require the measurement of the polarization of the leptons from the J/ψ decay [20]. This could be done in principle using $J/\psi \to \mu^+\mu^-$ decays or with $\psi(2S) \to \tau^+\tau^-$ decays by measuring the lepton polarizations. Such measurements are not feasible today. Theoretical arguments, based on the analysis of s-quark helicity conservation, suggest a "preferred" set of strong phases [21], but cannot guarantee the validity of this set.

In this analysis, we use the known dependence on $K\pi$ invariant mass of the relative phase between the S-wave and P-wave $K\pi$ $I = 1/2$ scattering amplitudes in the vicinity of the $K^*(892)$ to resolve the two-fold ambiguity in the relative strong phases among the three amplitudes for $B \to J/\psi K^*$. The dominant P-wave has the canonical Breit-Wigner form with a phase δ_P that increases rapidly with $K\pi$ invariant mass $m_{K\pi}$, while the S-wave phase δ_S increases slowly with $m_{K\pi}$ [22]. Accordingly, $\delta_S - \delta_P$, where δ_P is assumed to be common to the three $B \to J/\psi K\pi$ P-wave amplitudes, is expected to decrease rapidly as $m_{K\pi}$ increases from below to above the K^* resonance. We find that one solution for $\delta_S - \delta_P$ yields this expected behaviour while the other has precisely the opposite behavior. In this way, the ambiguity is resolved, so that the subsequent time-dependent analysis yields a value of $\cos 2\beta$ that is free of the associated sign ambiguity.

We perform an angular analysis of the $B \to J/\psi K^*$ decay mode and measure $\cos 2\beta$ on a sample of $(88 \pm 1) \times 10^6$ $B\overline{B}$ pairs collected with the *BABAR* detector at the PEP-II asymmetric-energy B Factory. These data correspond to an integrated luminosity of 81.9 fb^{-1} recorded at the $\Upsilon(4S)$ resonance. The analysis is performed in three distinct stages.

In the first stage the time-integrated angular distributions describing the decay channels $B^0 \to J/\psi K^{*0}, K^{*0} \to K^+\pi^-$ and $B^+ \to J/\psi K^{*+}, K^{*+} \to K_S^0\pi^+$ and $K^{*+} \to K^+\pi^0$, together with those of the related charge-conjugate modes, are analyzed assuming that the $K\pi$ system may be described entirely in terms of P-wave amplitudes. The weak process $b \to c\bar{c}s$ is a

*Also with Università della Basilicata, Potenza, Italy

†Also with IFIC, Instituto de Física Corpuscular, CSIC-Universidad de Valencia, Valencia, Spain

‡Deceased

TABLE I: The $B \to J/\psi K^*(892)$ amplitude parameters (described in Sec. I) as measured by several experiments. The results in Ref. [19] are superseded by this work. Note that the phases are subject to a two-fold ambiguity, as described by Eq. (4).

	$|A_0|^2$	$|A_\perp|^2$	$\delta_\parallel - \delta_0$ (rad)	$\delta_\perp - \delta_0$ (rad)
CLEO [23]	$0.52 \pm 0.07 \pm 0.04$	$0.16 \pm 0.08 \pm 0.04$	$3.00 \pm 0.37 \pm 0.04$	$-0.11 \pm 0.46 \pm 0.03$
CDF [24]	$0.59 \pm 0.06 \pm 0.01$	$0.13^{+0.12}_{-0.09} \pm 0.06$	$2.2 \pm 0.5 \pm 0.1$	$-0.6 \pm 0.5 \pm 0.1$
BABAR [19]	$0.597 \pm 0.028 \pm 0.024$	$0.160 \pm 0.032 \pm 0.014$	$2.50 \pm 0.20 \pm 0.08$	$-0.17 \pm 0.16 \pm 0.07$
Belle [25]	$0.617 \pm 0.020 \pm 0.027$	$0.192 \pm 0.023 \pm 0.026$	$2.83 \pm 0.19 \pm 0.08$	$-0.09 \pm 0.13 \pm 0.06$

$\Delta I = 0$ interaction, so the amplitudes for B^0 and B^+ decay should be equal, as should be those for $\overline{B}^0$ and B^-. A convenient description of the decays is provided in the transversity basis [14] since the related amplitudes have well-defined CP parities, which is of particular relevance for the $\cos 2\beta$ measurement. The formalism is described in Sec. I A and the results of its application to the data are presented in Sec. IV in the form of transversity-amplitude magnitudes and relative phases. There is an intrinsic mathematical ambiguity associated with the phases; the relevant transformation expressed in Eq. (4) below leaves the angular distribution unchanged.

This ambiguity can be resolved by extending the formalism to include a $K\pi$ S-wave amplitude and then measuring the $K\pi$ mass-dependence of its phase difference with respect to the P-waves. We will show that including a $K\pi$ S-wave with a significant S–P interference is required to describe the data (see Sec. V A). The extended angular distribution is presented in Sec. I B, and its use in resolving the phase ambiguity is described in Sec. V. This is the second stage in the analysis procedure.

The P-wave parameters extracted in Sec. IV are only slightly affected by the presence of an S-wave amplitude since in performing the analysis the data are integrated over a broad (± 100 MeV/c^2) $K\pi$ mass interval centered on the $K^*(892)$. The S–P interference contributions essentially average out over this region, and since the S-wave intensity proves to be only a few percent of that of the P-wave, the presence of the S-wave can be accounted for by a small additional source of systematic uncertainty (Table V, line 7).

The third stage of the analysis is the application of the time-dependent formalism to the $B^0 \to J/\psi K^{*0}(K_S^0 \pi^0)$ decay channel, as described in Sec. I C. There, the $K\pi$ S-wave is omitted and the P-wave parameters are fixed to those obtained during the first stage of the analysis. The phase ambiguity discussed in Sec. I A translates into a sign ambiguity for $\cos 2\beta$. The $K\pi$ S–P interference analysis of Sec. IV resolves the ambiguity and results in the assignment of a unique sign to the term in the time-dependent angular distribution that is proportional to $\cos 2\beta$. The time-dependent analysis of the $B^0 \to J/\psi K^{*0}(K_S^0 \pi^0)$ data sample, which is statistically independent of that used for the measurement of the amplitudes, is presented in Sec. VI. We summarize the results of the paper in Sec. VII.

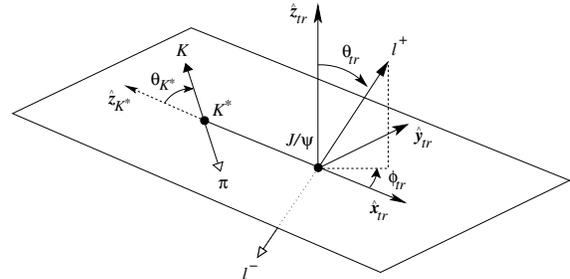Several experiments have determined the decay amplitudes in $B \to J/\psi K^*$ decay. These results are sum-

FIG. 1: Definition of the transversity angles $(\theta_{K^*}, \theta_{tr}, \phi_{tr})$ and coordinate system $(\hat{\boldsymbol{x}}_{tr}, \hat{\boldsymbol{y}}_{tr}, \hat{\boldsymbol{z}}_{tr})$. The direction opposite to the B meson momentum in the J/ψ rest frame is $\hat{\boldsymbol{x}}_{tr}$; $\hat{\boldsymbol{y}}_{tr}$ is perpendicular to $\hat{\boldsymbol{x}}_{tr}$ in the plane that contains $\hat{\boldsymbol{x}}_{tr}$ and $\vec{\boldsymbol{p}}_K$, chosen so $\vec{\boldsymbol{p}}_K \cdot \hat{\boldsymbol{y}}_{tr} > 0$; $\hat{\boldsymbol{z}}_{tr} = \hat{\boldsymbol{x}}_{tr} \times \hat{\boldsymbol{y}}_{tr}$. The helicity angle θ_{K^*} of the K^* decay is the angle between the direction opposite to the B meson flight direction and the kaon momentum, in the K^* rest frame. Finally, θ_{tr} and ϕ_{tr} are the polar and azimuthal angle of the positive lepton defined in the J/ψ rest frame.

marized in Table I. The measurements presented here supersede previous *BABAR* results [19], which are based on subsets of the data used for this analysis. The data reconstruction and Monte Carlo simulation procedures have undergone significant improvement since our previous analysis; the reconstruction of $J/\psi K^*$ channels involving a π^0 has been improved (Sec. III) leading to a better purity; a dedicated background subtraction method has been developed (Sec. IV B and Appendix A).

I. ANGULAR- AND TIME-DEPENDENT DIFFERENTIAL DECAY RATES

The B decay amplitudes are measured from the time-integrated differential decay distribution, expressed in the transversity basis. The definitions of the transversity frame and the related transversity angles $(\theta_{K^*}, \theta_{tr}, \phi_{tr})$ are shown in Fig. 1.

A. The Time-Integrated $J/\psi K^*$ Angular Distribution

We first consider only the $K^*(892)$ $K\pi$ mass region. The amplitude for longitudinal polarization of the two

vector mesons is A_0. There are two amplitudes for polarizations of the vector mesons transverse to the decay axis: $A_\parallel$ for parallel polarization of the two vector mesons and $A_\perp$ for their perpendicular polarization. The three independent amplitudes are assumed to have a common dependence on $m_{K\pi}$. This common dependence is irrelevant to the angular distribution and each of the three amplitudes is thus represented by a complex constant.

In terms of the angular variables $\boldsymbol{\omega} \equiv (\theta_{K^*}, \theta_{tr}, \phi_{tr})$, the time-integrated differential decay rate for the decay of the B meson to the $J/\psi\,(K^+\pi^-)_{P\text{-wave}}$, $J/\psi\,(K^+\pi^0)_{P\text{-wave}}$, or $J/\psi\,(K_s^0\pi^+)_{P\text{-wave}}$ final state is

$$
\begin{aligned}
g(\boldsymbol{\omega}; \boldsymbol{A}) &\equiv \frac{1}{\Gamma}\frac{\mathrm{d}^3\Gamma}{\mathrm{d}\cos\theta_{K^*}\mathrm{d}\cos\theta_{tr}\mathrm{d}\phi_{tr}} \\
&= f_1(\boldsymbol{\omega})|A_0|^2 + f_2(\boldsymbol{\omega})|A_\parallel|^2 + f_3(\boldsymbol{\omega})|A_\perp|^2 + \\
&\quad f_4(\boldsymbol{\omega})\Im m(A_\parallel^* A_\perp) + f_5(\boldsymbol{\omega})\Re e(A_\parallel A_0^*) + \\
&\quad f_6(\boldsymbol{\omega})\Im m(A_\perp A_0^*),
\end{aligned}
\tag{1}
$$

where the functions $f_i(\boldsymbol{\omega})$ are

$$
\begin{aligned}
f_1(\boldsymbol{\omega}) &\equiv \frac{9}{32\pi} 2\cos^2\theta_{K^*}\left[1 - \sin^2\theta_{tr}\cos^2\phi_{tr}\right], \\
f_2(\boldsymbol{\omega}) &\equiv \frac{9}{32\pi}\sin^2\theta_{K^*}\left[1 - \sin^2\theta_{tr}\sin^2\phi_{tr}\right], \\
f_3(\boldsymbol{\omega}) &\equiv \frac{9}{32\pi}\sin^2\theta_{K^*}\sin^2\theta_{tr}, \\
f_4(\boldsymbol{\omega}) &\equiv \frac{9}{32\pi}\sin^2\theta_{K^*}\sin 2\theta_{tr}\sin\phi_{tr}, \\
f_5(\boldsymbol{\omega}) &\equiv -\frac{9}{32\pi}\frac{1}{\sqrt{2}}\sin 2\theta_{K^*}\sin^2\theta_{tr}\sin 2\phi_{tr}, \\
f_6(\boldsymbol{\omega}) &\equiv \frac{9}{32\pi}\frac{1}{\sqrt{2}}\sin 2\theta_{K^*}\sin 2\theta_{tr}\cos\phi_{tr}.
\end{aligned}
\tag{2}
$$

Equations (1,2) have been obtained by summing over the unobserved lepton polarizations [20, 26, 27].

The symbol $\boldsymbol{A}$ denotes the transversity amplitudes for the decay of the B meson: $\boldsymbol{A} \equiv (A_0, A_\parallel, A_\perp)$. We set $|A_0|^2 + |A_\parallel|^2 + |A_\perp|^2 = 1$, so that $g(\boldsymbol{\omega}; \boldsymbol{A})$ (Eq. (1)) is a probability density function (PDF). We denote by $\overline{\boldsymbol{A}}$ the amplitudes for the $\overline{B}$ meson decay. In the absence of direct CP violation, we can choose a phase convention so that these amplitudes are related by $\overline{A}_0 = +A_0$, $\overline{A}_\parallel = +A_\parallel$, $\overline{A}_\perp = -A_\perp$, so that $A_\perp$ is CP-odd and A_0 and $A_\parallel$

are CP-even. Fixing this phase convention also fixes the phase of the amplitude for B^0–$\overline{B}^0$ mixing.

The phases δ_i of the amplitudes, where $i = 0, \parallel, \perp$, are defined by $A_i = |A_i|e^{i\delta_i}$. Obviously, only differences of phases appear in the differential decay rate through the observables

$$
\begin{aligned}
\Im m(A_\parallel^* A_\perp) &= |A_\parallel||A_\perp|\sin(\delta_\perp - \delta_\parallel), \\
\Re e(A_\parallel A_0^*) &= |A_\parallel||A_0|\cos(\delta_\parallel - \delta_0), \\
\Im m(A_\perp A_0^*) &= |A_\perp||A_0|\sin(\delta_\perp - \delta_0),
\end{aligned}
\tag{3}
$$

so that the differential decay rate (Eq.(1)) is invariant under the tranformation

$$
(\delta_\parallel - \delta_0, \delta_\perp - \delta_0) \longleftrightarrow (\delta_0 - \delta_\parallel, \pi + \delta_0 - \delta_\perp).
\tag{4}
$$

This is the above-mentioned ambiguity.

The three terms that would allow to resolve the ambiguity ($\Re e(A_\parallel^* A_\perp)$, $\Im m(A_\parallel A_0^*)$ and $\Re e(A_\perp A_0^*)$) vanish after summation over the unobserved final lepton polarizations.

We ensure $|A_0|^2 + |A_\parallel|^2 + |A_\perp|^2 = 1$ by parametrizing the magnitudes of the three B-decay amplitudes by

$$
\begin{aligned}
\cos\theta_A &\equiv |A_0|, \\
\sin\theta_A\cos\phi_A &\equiv |A_\parallel|, \\
\sin\theta_A\sin\phi_A &\equiv |A_\perp|.
\end{aligned}
\tag{5}
$$

with $0 \le \theta_A \le \pi/2$, $0 \le \phi_A \le \pi/2$.

B. Angular Distributions Including a $K\pi$ S-Wave Contribution

The $K\pi$ system originating from $B \to J/\psi\,(K\pi)$ can, in principle, have any integer spin. The experiment with the largest $K\pi$ sample, LASS [22], showed however that below 1.3 GeV/c^2, the S and P waves dominate. We have previously observed a broad structure [19] in the $1.1-1.3$ GeV/c^2 range of the $m_{K\pi}$ spectrum and found it to be compatible with a significant S-wave amplitude contribution. When a $K\pi$ S wave in the B decay amplitude is included in addition to the $K\pi$ P wave, the differential decay rate (Eq. (1)) becomes [27]

$$
\begin{aligned}
G_{S+P}(\boldsymbol{\omega}, m_{K\pi}; \boldsymbol{A}, A_P, A_S) &\equiv \frac{1}{\Gamma}\frac{\mathrm{d}^4\Gamma}{\mathrm{d}m_{K\pi}\mathrm{d}\cos\theta_{K^*}\mathrm{d}\cos\theta_{tr}\mathrm{d}\phi_{tr}} \\
&\propto pq \times \Bigg[A_P^2 g(\boldsymbol{\omega}; \boldsymbol{A}) + |A_S|^2 f_7(\boldsymbol{\omega}) + \\
&\quad A_P\left[f_8(\boldsymbol{\omega})\Re e\left(A_\parallel A_S^*\right) + f_9(\boldsymbol{\omega})\Im m\left(A_\perp A_S^*\right) + f_{10}(\boldsymbol{\omega})\Re e\left(A_0 A_S^*\right)\right]\Bigg],
\end{aligned}
\tag{6}
$$

where we have kept the notation θ_{K^*} for the $(K\pi)$ helicity angle; p is the $K\pi$-system momentum in the B rest frame and q is the kaon momentum in the $K\pi$ rest frame; we chose A_P to a be real and positive function of $m_{K\pi}$. Its square is indicative of the overall strength of the P-wave amplitudes. We represent the $m_{K\pi}$-dependent S-wave amplitude as $A_S = |A_S|e^{i\delta_S}$. The phases of the P-wave amplitudes reside in A_0, $A_\parallel$, and $A_\perp$.

Using the same phase convention as for the P-wave amplitudes, $\overline{A}_S = A_S$. The angular functions $f_{7\cdots10}$ are

$$f_7(\boldsymbol{\omega}) \equiv \frac{3}{32\pi}2\left[1 - \sin^2\theta_{tr}\cos^2\phi_{tr}\right],$$
$$f_8(\boldsymbol{\omega}) \equiv -\frac{3}{32\pi}\sqrt{6}\sin\theta_{K^*}\sin^2\theta_{tr}\sin 2\phi_{tr},$$
$$f_9(\boldsymbol{\omega}) \equiv \frac{3}{32\pi}\sqrt{6}\sin\theta_{K^*}\sin 2\theta_{tr}\cos\phi_{tr},$$
$$f_{10}(\boldsymbol{\omega}) \equiv \frac{3}{32\pi}4\sqrt{3}\cos\theta_{K^*}\left[1 - \sin^2\theta_{tr}\cos^2\phi_{tr}\right].$$
$$(7)$$

At a given $m_{K\pi}$, the normalization is obtained by introducing the parametrization

$$\cos\lambda \equiv \frac{A_P}{\sqrt{A_P^2 + |A_S|^2}},$$
$$\sin\lambda \equiv \frac{|A_S|}{\sqrt{A_P^2 + |A_S|^2}}, \qquad (8)$$

where λ is in the range $[0, \pi/2]$. The term $\cos^2\lambda$ $(\sin^2\lambda)$ represents the fraction of the P-wave (S-wave) intensity at that value of $m_{K\pi}$. The distribution (Eq. (6)), normalized so that at any fixed $m_{K\pi}$ the integral over the angular variables yields unity, is given by

$$g_{S+P}(\boldsymbol{\omega}; m_{K\pi}, \boldsymbol{A}, \lambda) \equiv \cos^2\lambda\, g(\boldsymbol{\omega}; \boldsymbol{A}) + \sin^2\lambda\, f_7(\boldsymbol{\omega})$$
$$+ \frac{1}{2}\sin 2\lambda\Big[$$
$$f_8(\boldsymbol{\omega})\cos(\delta_\parallel - \delta_S)|A_\parallel|$$
$$+ f_9(\boldsymbol{\omega})\sin(\delta_\perp - \delta_S)|A_\perp|$$
$$+ f_{10}(\boldsymbol{\omega})\cos(\delta_S - \delta_0)|A_0|\Big].$$
$$(9)$$

In Eq. (9), the dependence of g_{S+P} on $m_{K\pi}$ follows from that of λ and of the strong phases δ_i $(i =\perp, \parallel, 0, S)$. We see that at a given value of $m_{K\pi}$ the equations are invariant under the transformation

$$(\delta_\parallel - \delta_0, \delta_\perp - \delta_0, \delta_S - \delta_0) \longleftrightarrow$$
$$(\delta_0 - \delta_\parallel, \pi + \delta_0 - \delta_\perp, \delta_0 - \delta_S). \qquad (10)$$

We will use the change of the S–P relative phase in the region of the $K^*(892)$ to resolve this ambiguity.

The phase of a weak decay amplitude is determined by phases introduced through the weak interaction itself, that is from the CKM matrix, and by strong final-state interactions. If in the decay $B \to J/\psi K\pi$ the J/ψ were known not to interact with the $K\pi$ system, Watson's final-state interaction theorem [28] would guarantee that the phases for the P-wave and S-wave final states would be simply the corresponding phase shifts in P-wave and S-wave $K\pi$ scattering at the appropriate invariant mass, taking $K\pi$ scattering to be elastic in this range. However, we know this is not exactly the case, for if it were, the three individual P-wave amplitudes would be relatively real (relative phases 0 or π). This is not the experimental result, as we shall show. Nonetheless, we will provisionally adopt the assumption that the interactions with the J/ψ are small, and in particular that they do not change significantly with $m_{K\pi}$. We then anticipate that the difference $\delta_S - \delta_0$ will behave much like the difference $\delta(K\pi(L=0)) - \delta(K\pi(L=1))$, where we restrict ourselves to the $I = 1/2$ channel, which is produced in the $B \to J/\psi K\pi$ decay. According to Wigner's causality principle [29], the phase of a resonant amplitude increases with increasing invariant mass. Since the $K\pi$, $I = 1/2$ P-wave phase shift increases rapidly in the vicinity of the $K^*(892)$, while the corresponding S-wave increases only very gradually, we expect $\delta_S - \delta_0$, $\delta_S - \delta_\perp$, and $\delta_S - \delta_\parallel$ to fall rapidly with increasing $m_{K\pi}$ in this region.

C. Time-Dependent Angular Distribution

The time-dependent angular distribution for a B^0 meson produced at time $t = 0$ decaying as $B^0 \to J/\psi\ K^{*0}$ $(K^{*0} \to K_S^0\ \pi^0)$ at proper time t has the same form as in Eq. (1) but with time-dependent amplitudes $\boldsymbol{A}(t)$:

$$g(\boldsymbol{\omega}; \boldsymbol{A}(t), \sin 2\beta, \cos 2\beta) \equiv \frac{1}{\Gamma}\frac{\mathrm{d}^4\Gamma}{\mathrm{d}t\,\mathrm{d}\cos\theta_{K^*}\mathrm{d}\cos\theta_{tr}\mathrm{d}\phi_{tr}}. \qquad (11)$$

Under the hypothesis of no direct CP violation in the decay, i.e. $|A_i(0)| = |\overline{A}_i(0)|$, $i = 0, \parallel, \perp$, the corresponding terms that enter Eq. (11) are [16, 17, 27]

$$\left|\overset{(-)}{A_0}(t)\right|^2 \equiv e^{-\Gamma_0 t}|A_0|^2\left[1 \overset{(-)}{+} \sin 2\beta \sin \Delta m\,t\right],$$

$$\left|\overset{(-)}{A_\parallel}(t)\right|^2 \equiv e^{-\Gamma_0 t}|A_\parallel|^2\left[1 \overset{(-)}{+} \sin 2\beta \sin \Delta m\,t\right],$$

$$\left|\overset{(-)}{A_\perp}(t)\right|^2 \equiv e^{-\Gamma_0 t}|A_\perp|^2\left[1 \overset{(+)}{-} \sin 2\beta \sin \Delta m\,t\right],$$

$$\Im m\left(\overset{(-)^*}{A_\parallel}(t)\,\overset{(-)}{A_\perp}(t)\right) \equiv \overset{(-)}{+} e^{-\Gamma_0 t}|A_\parallel||A_\perp|\left[\sin(\delta_\perp - \delta_\parallel)\cos\Delta m\,t - \cos(\delta_\perp - \delta_\parallel)\cos 2\beta \sin\Delta m\,t\right],$$

$$\Re e\left(\overset{(-)}{A_\parallel}(t)\,\overset{(-)^*}{A_0}(t)\right) \equiv e^{-\Gamma_0 t}|A_\parallel||A_0|\,\cos(\delta_\parallel - \delta_0)\left[1 \overset{(-)}{+} \sin 2\beta \sin\Delta m\,t\right],$$

$$\Im m\left(\overset{(-)}{A_\perp}(t)\,\overset{(-)^*}{A_0}(t)\right) \equiv \overset{(-)}{+} e^{-\Gamma_0 t}|A_\perp||A_0|\left[\sin(\delta_\perp - \delta_0)\cos\Delta m\,t - \cos(\delta_\perp - \delta_0)\cos 2\beta \sin\Delta m\,t\right], \tag{12}$$

for an initial B^0 $(\overline{B}^0)$ meson. The mass difference between the two neutral B mass eigenstates is Δm, and Γ_0 is the common neutral B-meson decay rate, neglecting the lifetime difference between these mass eigenstates. The expression for the differential decay rate can be recast in the following form [27]:

$$g_\eta(\boldsymbol{\omega}, t; \boldsymbol{A}, \sin 2\beta, \cos 2\beta) = \frac{\Gamma_0}{2}e^{-\Gamma_0 t}\mathcal{A}(\boldsymbol{\omega}; \boldsymbol{A}) \times$$
$$\left\{1 + \eta\left[\cos\Delta m\,t\,\frac{\mathcal{P}(\boldsymbol{\omega}; \boldsymbol{A})}{\mathcal{A}(\boldsymbol{\omega}; \boldsymbol{A})} + \sin\Delta m\,t\left(\frac{\mathcal{S}(\boldsymbol{\omega}; \boldsymbol{A})}{\mathcal{A}(\boldsymbol{\omega}; \boldsymbol{A})}\sin 2\beta + \frac{\mathcal{C}(\boldsymbol{\omega}; \boldsymbol{A})}{\mathcal{A}(\boldsymbol{\omega}; \boldsymbol{A})}\cos 2\beta\right)\right]\right\}, \tag{13}$$

with $\eta = +1$ ($\eta = -1$) for an initial B^0 $(\overline{B}^0)$ meson. The angular terms $\mathcal{A}$, $\mathcal{P}$, $\mathcal{S}$, and $\mathcal{C}$ are

$$\begin{aligned}
\mathcal{A}(\boldsymbol{\omega}; \boldsymbol{A}) &\equiv& f_1(\boldsymbol{\omega})|A_0|^2 + f_2(\boldsymbol{\omega})|A_\parallel|^2 + f_3(\boldsymbol{\omega})|A_\perp|^2 + f_5(\boldsymbol{\omega})|A_0||A_\parallel|\cos(\delta_\parallel - \delta_0),\\
\mathcal{P}(\boldsymbol{\omega}; \boldsymbol{A}) &\equiv& f_4(\boldsymbol{\omega})|A_\parallel||A_\perp|\sin(\delta_\perp - \delta_\parallel) + f_6(\boldsymbol{\omega})|A_0||A_\perp|\sin(\delta_\perp - \delta_0),\\
\mathcal{S}(\boldsymbol{\omega}; \boldsymbol{A}) &\equiv& f_1(\boldsymbol{\omega})|A_0|^2 + f_2(\boldsymbol{\omega})|A_\parallel|^2 - f_3(\boldsymbol{\omega})|A_\perp|^2 + f_5(\boldsymbol{\omega})|A_0||A_\parallel|\cos(\delta_\parallel - \delta_0),\\
\mathcal{C}(\boldsymbol{\omega}; \boldsymbol{A}) &\equiv& -f_4(\boldsymbol{\omega})|A_\parallel||A_\perp|\cos(\delta_\perp - \delta_\parallel) - f_6(\boldsymbol{\omega})|A_0||A_\perp|\cos(\delta_\perp - \delta_0).
\end{aligned} \tag{14}$$

The time-dependent asymmetry in the decay then reads

$$\begin{aligned}
a(\boldsymbol{\omega}, t; \boldsymbol{A}, \sin 2\beta, \cos 2\beta) &\equiv& \frac{g_{+1}(\boldsymbol{\omega}, t; \boldsymbol{A}, \sin 2\beta, \cos 2\beta) - g_{-1}(\boldsymbol{\omega}, t; \boldsymbol{A}, \sin 2\beta, \cos 2\beta)}{g_{+1}(\boldsymbol{\omega}, t; \boldsymbol{A}, \sin 2\beta, \cos 2\beta) + g_{-1}(\boldsymbol{\omega}, t; \boldsymbol{A}, \sin 2\beta, \cos 2\beta)}\\
&=& \cos\Delta m\,t\,\frac{\mathcal{P}(\boldsymbol{\omega}; \boldsymbol{A})}{\mathcal{A}(\boldsymbol{\omega}; \boldsymbol{A})} + \sin\Delta m\,t\left(\frac{\mathcal{S}(\boldsymbol{\omega}; \boldsymbol{A})}{\mathcal{A}(\boldsymbol{\omega}; \boldsymbol{A})}\sin 2\beta + \frac{\mathcal{C}(\boldsymbol{\omega}; \boldsymbol{A})}{\mathcal{A}(\boldsymbol{\omega}; \boldsymbol{A})}\cos 2\beta\right). \tag{15}
\end{aligned}$$

This reduces to the usual expression for decays to CP eigenstates when only the CP-even (A_0, $A_\parallel$) amplitudes are nonzero or when only the CP-odd ($A_\perp$) amplitude is nonzero. We now examine the terms on the right hand side of Eq. (15):

- The $\cos\Delta m\,t$ term makes the smallest contribution to $g_\eta(\boldsymbol{\omega}, t; \boldsymbol{A}, \sin 2\beta, \cos 2\beta)$ because the distribution of values taken by $\mathcal{P}(\boldsymbol{\omega}; \boldsymbol{A})/\mathcal{A}(\boldsymbol{\omega}; \boldsymbol{A})$, as shown in Fig. 2(a), peaks at zero.

- The $\sin\Delta m\,t$ term has explicit dependence on both

$\sin 2\beta$ and $\cos 2\beta$:

  ○ The usual $\sin(\Delta mt)\sin 2\beta$ factor is weighted by the angular term $\mathcal{S}(\boldsymbol{\omega}; \boldsymbol{A})/\mathcal{A}(\boldsymbol{\omega}; \boldsymbol{A})$, which can take values between -1 and $+1$, and whose distribution is shown in Fig. 2(b). This distribution reduces to one peak at $+1$ or -1 for a pure CP-even ($|A_\perp| = 0$) or CP-odd ($|A_\perp| = 1$) decay, respectively.

  ○ The $\cos 2\beta$ contribution is characteristic of a vector-vector channel. This contribution appears only *via* the interference terms involving
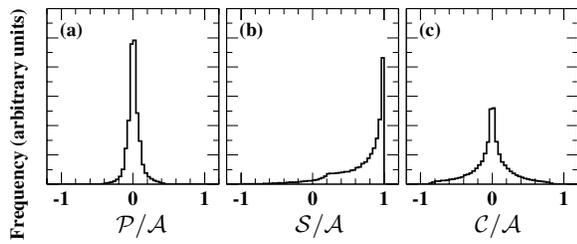
FIG. 2: (a) The distribution of $\mathcal{P}(\boldsymbol{\omega};\boldsymbol{A})/\mathcal{A}(\boldsymbol{\omega};\boldsymbol{A})$, (b) $\mathcal{S}(\boldsymbol{\omega};\boldsymbol{A})/\mathcal{A}(\boldsymbol{\omega};\boldsymbol{A})$ and (c) $\mathcal{C}(\boldsymbol{\omega};\boldsymbol{A})/\mathcal{A}(\boldsymbol{\omega};\boldsymbol{A})$, where $\mathcal{A}$, $\mathcal{P}$, $\mathcal{S}$ and $\mathcal{C}$ are defined by Eq. (14), for a set of events generated according to the amplitudes $\boldsymbol{A}$ corresponding to the *BABAR* values in Table I.

the *CP*-odd amplitude $A_\perp$ and the *CP*-even amplitudes A_0 and $A_\parallel$ (Eq. (14)). The angular term $\mathcal{C}(\boldsymbol{\omega};\boldsymbol{A})/\mathcal{A}(\boldsymbol{\omega};\boldsymbol{A})$ takes values in a range smaller than $[-1,+1]$ (Fig. 2(c)), whose bounds depend on the amplitudes and phases. The distribution of this angular term tends to peak at zero (Fig. 2(c)), inducing some loss in sensitivity to $\cos 2\beta$ compared to that to $\sin 2\beta$.

○ The $\sin 2\beta$ and $\cos 2\beta$ contributions are distinguished by the angular information only.

○ From the orthogonality of the angular functions $\mathcal{S}$ and $\mathcal{C}$ (Eq. (14)) and the angular symmetry of g_η (Eq. (13)), the $\sin 2\beta$ and $\cos 2\beta$ parameters, if regarded as independent quantities, are uncorrelated in a fit of the differential decay rate (Eq. (13)), in the limit of infinite statistics and in the absence of experimental effects.

Under the transformation $(\delta_\parallel - \delta_0, \delta_\perp - \delta_0) \rightarrow (\delta_0 - \delta_\parallel, \pi + \delta_0 - \delta_\perp)$, $\mathcal{A}$, $\mathcal{P}$, and $\mathcal{S}$ are unchanged, while $\mathcal{C}$ changes sign, showing that the ambiguity in the strong phases translates into an ambiguity in the sign of $\cos 2\beta$:

$$\left(\delta_\parallel - \delta_0, \delta_\perp - \delta_0, \cos 2\beta\right) \longleftrightarrow$$
$$\left(\delta_0 - \delta_\parallel, \pi + \delta_0 - \delta_\perp, -\cos 2\beta\right). \qquad (16)$$

II. THE *BABAR* DETECTOR

A detailed description of the *BABAR* detector is presented in Ref. [30]. Charged particles are detected with a five-layer, double-sided silicon vertex tracker (SVT) and a 40-layer drift chamber (DCH) with a helium-isobutane gas mixture, placed in a 1.5-T solenoidal field produced by a superconducting magnet. The charged-particle momentum resolution is approximately $(\delta p_T/p_T)^2 = (0.0013\,p_T)^2 + (0.0045)^2$, where p_T is the transverse momentum in GeV/c. The SVT, with a typical single-hit resolution of $10\,\mu$m, measures the impact parameters of charged-particle tracks in both the plane transverse to the beam direction and along the beam.

Charged-particle types are identified from the ionization energy loss (dE/dx) measured in the DCH and SVT, and from the Cherenkov radiation detected in a ring-imaging Cherenkov device. Photons are detected by a CsI(Tl) electromagnetic calorimeter (EMC) with an energy resolution $\sigma(E)/E = 0.023 \cdot (E/\,\text{GeV})^{-1/4} \oplus 0.019$. The return yoke of the superconducting coil is instrumented with resistive plate chambers (IFR) for the identification and muons and the detection of neutral hadrons.

III. EVENT RECONSTRUCTION AND SELECTION

The event selection is similar to that used in our previous analysis [19]. Multihadron events are selected by demanding a minimum of three reconstructed charged tracks in the polar angle range $0.41 < \theta_{lab} < 2.54$ rad. A charged track must be reconstructed in the DCH, and, if it does not result from a K_S^0 decay, it must originate at the nominal interaction point within 1.5 cm in the plane transverse to the beam and 10 cm along the beam. Events are required to have a primary vertex within 0.5 cm of the average position of the interaction point in the plane transverse to the beamline, and within 6 cm longitudinally. Electromagnetic depositions in the calorimeter in the polar angle range $0.410 < \theta_{lab} < 2.409$ rad that are not associated with charged tracks, that have an energy greater than 30 MeV and that have a shower shape consistent with a photon interaction are taken as neutral clusters. We require the total energy for charged tracks and photon candidates in the fiducial region to be greater than 4.5 GeV. To reduce continuum background, we require the normalized second Fox-Wolfram moment R_2 [31] of the event, calculated with both charged tracks and neutral clusters, to be less than 0.5.

Charged tracks are required to be in regions of polar angle for which the particle identification (PID) efficiency is well-measured. For electrons, muons, and kaons the acceptable ranges are 0.40 to 2.40, 0.30 to 2.70, and 0.45 to 2.50 rad, respectively.

Candidates for J/ψ mesons are reconstructed in the e^+e^- and $\mu^+\mu^-$ decay modes, from a pair of identified leptons that form a good vertex. A `Loose` [32] identification condition is required for each muon. (The number of interaction lengths it traverses in the EMC and IFR must be consistent with the expectation, as must be the average number of hits in each layer of the IFR; the IFR hits and the track extrapolation must match; the energy deposition in the EMC must be small.) A `Tight` condition [32] is required for each electron. (The measured dE/dx must be consistent with expectations; the energy deposition in the calorimeter must be consistent with the momentum measured in the drift chamber, and the lateral shower shape must be consistent with an electromagnetic shower.) Electrons that have no EMC information are selected on the basis of dE/dx information alone. For $J/\psi \rightarrow e^+e^-$ decays, where an electron may have radi-

ated one or several Bremsstrahlung photons, the missing energy is recovered by identifying EMC clusters with energy greater than 30 MeV lying within 35 mrad in polar angle and 50 mrad in azimuth of the electron direction projected onto the EMC. The lepton-pair invariant mass must be between 3.06 and 3.14 GeV/c^2 for muons, and between 2.95 and 3.14 GeV/c^2 for electrons. This corresponds to a $\pm 3\sigma$ interval for muons, and accounts for the partially recovered radiative tail due to Bremsstrahlung for electrons.

A candidate K_s^0 consists of a vertexed pair of oppositely-charged tracks with invariant mass between 489 and 507 MeV/c^2, when interpreted as pions. The K_s^0 flight length must be greater than 1 mm, and its direction must form an angle with the K_s^0 momentum vector in the plane perpendicular to the beam line that is less than 0.2 rad.

Neutral clusters, as defined above, are used as photon candidates for the reconstruction of $\pi^0 \to \gamma\gamma$ decays. A π^0 candidate consists of a pair of photons with invariant mass in the interval 106 to 153 MeV/c^2, and a total energy greater than 200 MeV.

The J/ψ, K_s^0, and π^0 candidates are constrained to their corresponding nominal masses. Except in the analysis that includes an S-wave contribution, K^* candidates must have a $K\pi$ invariant mass within 100 MeV/c^2 of the nominal $K^*(892)$ mass.

The J/ψ and K^* candidates are combined to form $B \to J/\psi K^*$ candidates. It may happen that a genuine $J/\psi K^*$ event is reconstructed incorrectly, most often with the true J/ψ, but with a wrongly reconstructed K^*. This happens mainly for B candidates with a daughter π^0, with cross-feed (CF) from the companion channel with a $\pi^\pm$, or self cross-feed (SCF) when the genuine π^0 is incorrectly reconstructed with at least one wrong photon candidate. The (S)CF is reduced by demanding, for channels with a π^0 in the final state, that $\cos\theta_{K^*} < 0.7$, where θ_{K^*} is the K^*-decay helicity angle (see Fig. 1). In addition, as was done in Ref. [27], if a single event can be reconstructed in two different K^* modes and if one reconstruction uses a π^0 and the other does not, the reconstruction without a π^0 is retained. This reduces the cross-feed by 75% for a 1% relative loss in signal efficiency. In modes with a $\pi^\pm$, no $\cos\theta_{K^*}$ cut is applied.

Two kinematic variables are used to further discriminate against incorrect B candidates. The first is the difference $\Delta E = E_B^* - E_{\text{beam}}^*$ between the candidate-B energy and the beam energy in the $\Upsilon(4S)$ rest frame. In the absence of experimental effects, reconstructed signal candidates have $\Delta E = 0$. The second is the beam-energy-substituted mass $m_{\text{ES}} = (E_{\text{exp}}^2 - \vec{p}_B^2)^{1/2}$ where, in the laboratory frame $E_{\text{exp}} = (s/2 + \vec{p}_B.\vec{p}_i)/E_i$ is the B-candidate expected energy, $\vec{p}_B$, its measured momentum, $(E_i, \vec{p}_i)$, the e^+e^- initial-state four-momentum, and $\sqrt{s}$ is the center-of-mass energy. For the signal region, ΔE is required to be between -70 MeV and $+50$ MeV for channels involving a π^0, and within 30 MeV of zero otherwise. If several B candidates are found in an event, the one

TABLE II: Event yield and purity, estimated from a fit to the m_{ES} distribution (Fig. 3), with a Gaussian signal distribution and an ARGUS threshold function [33] describing the combinatorial background. The spectra are integrated over the range $m_{\text{ES}} > 5.27$ GeV/c^2. No correction for cross-feed is made since these numbers are not used in the actual analysis; rather they provide an indication of the purity of the data sample.

Channel	Yield	Purity (%)
$J/\psi\,(K_s^0\pi^0)$	131 ± 14	81.6
$J/\psi\,(K^\pm\pi^\mp)$	2376 ± 51	95.8
$J/\psi\,(K_s^0\pi^\pm)$	670 ± 27	95.7
$J/\psi\,(K^\pm\pi^0)$	791 ± 33	85.0

with the smallest $|\Delta E|$ is retained.

The m_{ES} distributions for the $B \to J/\psi K\pi$ candidates are shown in Fig. 3. Corresponding signal yields and purities are given in Table II. These results are obtained from fits to the m_{ES} distributions using a Gaussian distribution for the signal and an ARGUS shape [33] for the combinatorial background of the form

$$a(m_{\text{ES}}) = a_0 m_{\text{ES}} \sqrt{1 - (m_{\text{ES}}/m_0)^2} \times \\ {}_\text{e}\xi\left(1 - (m_{\text{ES}}/m_0)^2\right),$$

(17)

for $m_{\text{ES}} < m_0$, where m_0 represents the kinematic upper limit and is fixed at the center-of-mass beam energy $E_{\text{beam}}^* = 5.291$ GeV. The parameter ξ determines the shape of the spectrum.

With the signal region defined by $m_{\text{ES}} > 5.27$ GeV/c^2 and the above ΔE ranges, the B reconstruction efficiencies, summed over $J/\psi \to e^-e^-$ and $J/\psi \to \mu^+\mu^-$, are $(9.6 \pm 0.1)\%$, $(24.5 \pm 0.1)\%$, $(19.7 \pm 0.2)\%$, and $(12.5 \pm 0.2)\%$ for the modes $K_s^0\,\pi^0$, $K^\pm\,\pi^\mp$, $K_s^0\,\pi^\pm$, and $K^\pm\,\pi^0$, respectively. The composition of the remaining background events is given in Table III. The contribution of B candidates with a fake J/ψ candidate is less than 2%.

IV. ANGULAR ANALYSIS

The parameters θ_A, ϕ_A (Eq. (5)), $\delta_\parallel - \delta_0$ and $\delta_\perp - \delta_0$ of the angular-dependent time-integrated decay rates are determined using a simultaneous unbinned likelihood fit to the three flavor-eigenstate $B \to J/\psi K^*$ channels: $J/\psi(K^\pm\pi^\mp)$, $J/\psi(K_s^0\pi^\pm)$, and $J/\psi(K^\pm\pi^0)$. The PDF, before accounting for the experimental effects described below, is given by Eq. (1). We first consider only the P-wave amplitudes; the effect of the S-wave amplitude is discussed in Sec. IV D. The B flavor is taken into account in the fit through the relations ($\overline{A}_0 = A_0$, $\overline{A}_\parallel = A_\parallel$, $\overline{A}_\perp = -A_\perp$) as explained in Sec. I.

TABLE III: The expected number of background events for each decay mode in the signal region, in an on-peak 81.9 fb^{-1} sample. The contribution from continuum is estimated using a 9.6 fb^{-1} off-peak data sample. The $B\overline{B}$ contribution is estimated using a fully-simulated sample of generic $B\overline{B}$ decays equivalent to 72 fb^{-1} (with the inclusive J/ψ events removed from the sample). The inclusive J/ψ contribution is estimated using a fully-simulated sample equivalent to 91 fb^{-1} ($B \to J/\psi K^*(892)$ events removed).

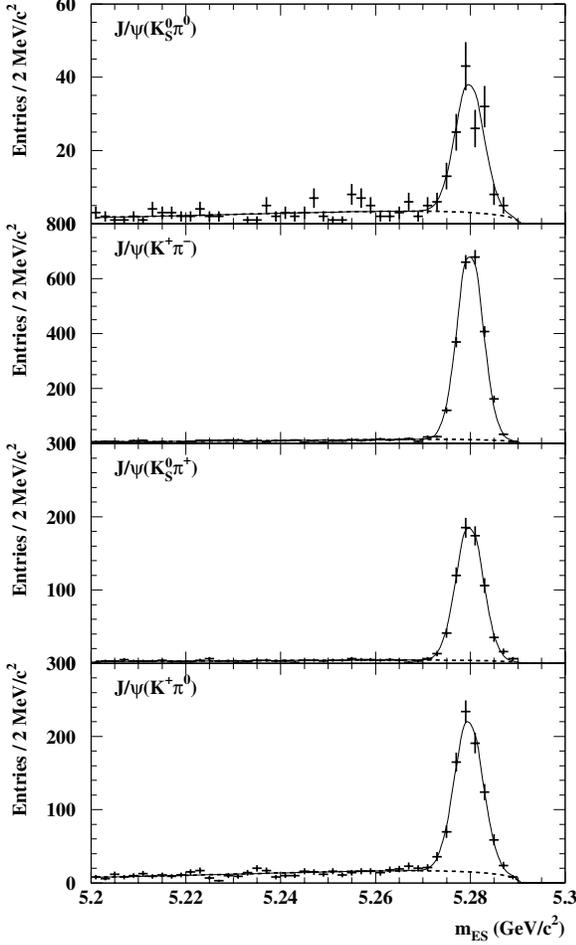| Background	B Decay Mode			
Source	$J/\psi\,(K_S^0\pi^0)$	$J/\psi\,(K^\pm\pi^\mp)$	$J/\psi\,(K_S^0\pi^\pm)$	$J/\psi\,(K^\pm\pi^0)$
Continuum	0.2 ± 0.1	1.2 ± 0.4	0.1 ± 0.1	0.7 ± 0.4
Generic $B\overline{B}$	0.2 ± 0.1	1.2 ± 0.2	0.3 ± 0.1	1.2 ± 0.3
Inclusive J/ψ	22 ± 5	126 ± 12	38 ± 7	135 ± 12

FIG. 3: The $m_{\rm ES}$ distributions for the ΔE intervals described in the text with overlaid Gaussian and ARGUS fit functions, for $J/\psi\,K\pi$ candidates in data.

A. Acceptance Correction

The acceptance correction is applied as in our previous measurement [19]. We perform an unbinned likelihood fit

of the PDF g^{obs} to the observed events, where

$$g^{obs}(\boldsymbol{\omega}; \boldsymbol{A}) = g(\boldsymbol{\omega}; \boldsymbol{A})\frac{\varepsilon(\boldsymbol{\omega})}{\langle\varepsilon\rangle(\boldsymbol{A})}, \qquad (18)$$

where $g(\boldsymbol{\omega}; \boldsymbol{A})$ is given by Eq. (1), $\varepsilon(\boldsymbol{\omega})$ is the angle-dependent acceptance, and

$$\langle\varepsilon\rangle(\boldsymbol{A}) \equiv \int g(\boldsymbol{\omega}; \boldsymbol{A})\varepsilon(\boldsymbol{\omega})\mathrm{d}\boldsymbol{\omega} \qquad (19)$$

is the average acceptance over the event-weighted phase space, which depends on the amplitudes $\boldsymbol{A}$, and which ensures the normalization of g^{obs}.

In the case of the $J/\psi K^*$ channels studied here, the presence of cross-feed from the companion channels, which have, as a consequence of isospin symmetry, the same $\boldsymbol{A}$ dependence as that of the signal, must be taken into account. The observed PDF for channel b ($b = K^\pm\pi^\mp, K_S^0\pi^\pm, K^\pm\pi^0$) is then

$$g^{b,obs}(\boldsymbol{\omega}; \boldsymbol{A}) = g(\boldsymbol{\omega}; \boldsymbol{A})\frac{\varepsilon^b(\boldsymbol{\omega})}{\sum_k \mathcal{A}_k(\boldsymbol{A})\Phi_k^b}, \qquad (20)$$

with

$$\varepsilon^b(\boldsymbol{\omega}) \equiv \sum_a F_a\,\varepsilon^{a\to b}(\boldsymbol{\omega}), \qquad (21)$$

$$\Phi_k^b \equiv \sum_a F_a \int f_k(\boldsymbol{\omega})\varepsilon^{a\to b}(\boldsymbol{\omega})\mathrm{d}\boldsymbol{\omega} \qquad (22)$$

and $a = K_S^0\pi^0, K^\pm\pi^\mp, K_S^0\pi^\pm, K^\pm\pi^0$. In the above expressions, the $\mathcal{A}_{1\ldots 6}$ terms are (see Eq.(1))

$$
\begin{aligned}
\mathcal{A}_1 &= |A_0|^2, \\
\mathcal{A}_2 &= |A_\parallel|^2, \\
\mathcal{A}_3 &= |A_\perp|^2, \\
\mathcal{A}_4 &= \Im m(A_\parallel^* A_\perp), \\
\mathcal{A}_5 &= \Re e(A_0^* A_\parallel), \\
\mathcal{A}_6 &= \Im m(A_0^* A_\perp),
\end{aligned} \qquad (23)
$$

and F_a is the fraction of mode a in $B \to J/\psi K^*$ decays (with $\sum_a F_a = 1$). We assume that $\mathcal{B}(\Upsilon(4S) \to B^0\overline{B}^0) = \mathcal{B}(\Upsilon(4S) \to B^+B^-)$, $\Gamma(K^{*0} \to K^+\pi^-) = 2 \times \Gamma(K^{*0} \to K^0\pi^0)$, and $\Gamma(K^{*+} \to K^0\pi^+) = 2 \times \Gamma(K^{*+} \to K^+\pi^0)$.

The measured values [34] of the branching fractions for the decays $B^0 \to J/\psi K^{*0}$ and $B^+ \to J/\psi K^{*+}$ are used. The angular functions $f_k(\boldsymbol{\omega})$ ($k = 1 \ldots 6$) have been defined in Eq. (2) and $\varepsilon^{a \to b}(\boldsymbol{\omega})$ is the probability for an event generated in channel a and with angles $\boldsymbol{\omega}$ to be detected as an event in channel b. Finally, $\varepsilon^b(\boldsymbol{\omega})$ is the efficiency for reconstructed channel b considering $B \to J/\psi K^*$ channels as a whole, that is counting cross-feed events as signal. The Φ_k^b are the $f_k(\boldsymbol{\omega})$ moments of the "whole" efficiency ε^b.

The angular resolution has been neglected, even for (self)cross-feed events. Also the possibility of doubly misidentifying the daughters of the $K^{*0} \to K^+\pi^-$ candidate (K–π swap) is not taken into account. The induced biases have been estimated with Monte Carlo (MC) based studies, and found to be negligible. Under these two approximations, the acceptance $\varepsilon^b(\boldsymbol{\omega})$ can be factorized as in Eq. (20), and only the coefficients Φ_k^b are needed.

The coefficients Φ_k^b are computed with exclusive signal MC samples obtained using a full simulation of the experiment [35–37]. Particle identification efficiencies measured with data control samples are used to adjust the MC simulation to represent the actual behavior of the detector. Separate coefficients are used for different charges of the final state mesons, in particular to take into account the charge dependence of the interaction of charged kaons with matter, and any other possible charge asymmetry of the detector. Writing the log-likelihood function for a pure signal sample we have, for each channel b,

$$
\begin{aligned}
L^b(\boldsymbol{A}) &\equiv \sum_{i=1}^{N_{evt}} \ln\left(g^{b,obs}(\boldsymbol{\omega}_i; \boldsymbol{A})\right) \\
&= \sum_{i=1}^{N_{evt}} \ln\left(g(\boldsymbol{\omega}_i; \boldsymbol{A})\right) - N_{evt} \ln\left(\sum_k \mathcal{A}_k(\boldsymbol{A})\Phi_k^b\right) \\
&\quad + \sum_{i=1}^{N_{evt}} \ln\left(\varepsilon^b(\boldsymbol{\omega}_i)\right).
\end{aligned}
\tag{24}
$$

where $\boldsymbol{\omega}_i$ represents the measured angular variables for event i, and N_{evt} is the total number of signal candidates. When maximizing $L^b(\boldsymbol{A})$, the third term, which does not depend on the amplitudes, can be ignored [19].

B. Background Subtraction

In our previous measurement [19] of the decay amplitudes, it was assumed that the combinatorial background could be taken into account with an expansion in the same basis functions as the signal. The systematic bias due to neglecting the missing components of the background angular distribution was checked with MC-based studies.

Here, we use an improved background correction method in which events from the m_{ES} sideband are added to the log-likelihood that is maximized, but with a negative weight.

The sample of N_{evt} events selected in the signal region contains n_S signal events and n_B background events, so that $N_{evt} = n_S + n_B$. The values of n_S and n_B are unknown *a priori*. The quantity we would like to maximize is $\sum_{i=1}^{n_S} \ln\left(g^{b,obs}(\boldsymbol{\omega}_i; \boldsymbol{A})\right)$, while we have

$$
\begin{aligned}
L^b(\boldsymbol{A}) &\equiv \sum_{i=1}^{N_{evt}} \ln\left(g^{b,obs}(\boldsymbol{\omega}_i; \boldsymbol{A})\right) \\
&= \sum_{i=1}^{n_S} \ln\left(g^{b,obs}(\boldsymbol{\omega}_i; \boldsymbol{A})\right) \\
&\quad + \sum_{j=1}^{n_B} \ln\left(g^{b,obs}(\boldsymbol{\omega}_j; \boldsymbol{A})\right).
\end{aligned}
\tag{25}
$$

Note that the same PDF appears for both the signal events and the background events: the PDF $g^{b,obs}$ of the signal. We use a pure sample of background events to obtain an estimate of the second term. This sample is from the m_{ES} sideband region $5.20 < m_{\mathrm{ES}} < 5.27\,\mathrm{GeV}/c^2$, which contains N_B events. It can be shown that maximizing the modified expression $L^{b\prime}$, where

$$
\begin{aligned}
L^{b\prime}(\boldsymbol{A}) &\equiv \sum_{i=1}^{N_{evt}} \ln(g^{b,obs}(\boldsymbol{\omega}_i; \boldsymbol{A})) \\
&\quad - \frac{\tilde{n}_B}{N_B} \sum_{k=1}^{N_B} \ln(g^{b,obs}(\boldsymbol{\omega}_k; \boldsymbol{A})) \\
&= \sum_{i=1}^{n_S} \ln(g^{b,obs}(\boldsymbol{\omega}_i; \boldsymbol{A})) + \sum_{j=1}^{n_B} \ln(g^{b,obs}(\boldsymbol{\omega}_j; \boldsymbol{A})) \\
&\quad - \frac{\tilde{n}_B}{N_B} \sum_{k=1}^{N_B} \ln(g^{b,obs}(\boldsymbol{\omega}_k; \boldsymbol{A})),
\end{aligned}
\tag{26}
$$

yields an unbiased estimator of the true parameters if $\tilde{n}_B$ is an unbiased estimator of n_B. The quantity $\tilde{n}_B$ is obtained by fitting the data from the m_{ES} sideband and signal regions with a combination of an ARGUS and a Gaussian function. Since there is no peaking background contribution in the signal region, we take for $\tilde{n}_B$ the portion of the ARGUS fit that falls in the signal region.

As $L^{b\prime}$ is not a log-likelihood, the uncertainties yielded by the minimization program `Minuit` [38] are biased estimates of the actual uncertainties. An unbiased estimation of the uncertainties is described and validated in Appendix A.

With this pseudo-log-likelihood technique, we avoid parametrizing the acceptance as well as the background angular distributions. This technique and the combined (m_{ES}, angular) likelihood fit used in Ref. [19] rely on the assumption that the angular behavior of the combinatorial background is the same in the m_{ES} signal region and sideband. The possible bias related to this assumption is discussed in the next section.

TABLE IV: Bias (in units of 10^{-3}) observed in fits for the individual K^* channels and the combined channel, based on parametrized Monte Carlo, taking as input the values of the amplitudes from Ref. [19]. The upper part of the table presents results for the fitted quantities $\theta_A, \phi_A, \delta_\parallel - \delta_0$, and $\delta_\perp - \delta_0$, all expressed in radians. The lower part presents results for the amplitude moduli squared, which are computed from θ_A and ϕ_A.

| | Bias (10^{-3}) | | | |
	$K^\pm \pi^\mp$	$K^0_S \pi^\pm$	$K^\pm \pi^0$	all K^*
θ_A	2.9 ± 1.0	-1.3 ± 1.9	-8.7 ± 1.9	-0.2 ± 0.8
ϕ_A	3.3 ± 3.5	13.0 ± 6.6	5.5 ± 6.4	5.5 ± 2.8
$\delta_\parallel - \delta_0$	-34.9 ± 7.8	-19.2 ± 14.7	-54.5 ± 13.9	-36.2 ± 6.2
$\delta_\perp - \delta_0$	-29.3 ± 6.4	-7.8 ± 11.8	-29.0 ± 11.4	-25.2 ± 5.0
$|A_0|^2$	-2.9 ± 1.0	1.3 ± 1.9	8.5 ± 1.9	0.2 ± 0.8
$|A_\parallel|^2$	0.4 ± 1.5	-5.9 ± 2.8	-7.2 ± 2.7	-2.2 ± 1.2
$|A_\perp|^2$	2.5 ± 1.4	4.6 ± 2.7	-1.3 ± 2.6	2.1 ± 1.1

C. Validation

The complete fit scheme, including acceptance and background corrections as described above, has been validated with a $B\overline{B}$ Monte Carlo sample equivalent to an integrated luminosity of 590 fb^{-1}, produced with a full simulation of the *BABAR* detector (based on GEANT4 [35–37]). In this sample only events with a true $J/\psi \to \ell\ell$ decay with center-of-mass momentum $p^*_{J/\psi}$ greater than 1.3 GeV/c are simulated. This momentum cut is not applied in the analysis. It does not affect the signal region ($m_{\rm ES} > 5.27\,{\rm GeV}/c^2$), but means that only a subset of the events in the $m_{\rm ES}$ sideband region is included.

An additional study has been performed with a larger sample generated with a parametrized simulation from the same event generator [35] with resolution effects and efficiencies incorporated. The equivalent integrated luminosity of this sample is 16 ab^{-1}.

The results of the two simulations are found to be compatible with each other. No statistically significant bias is observed with the full simulation. However, the high-statistics fast simulation shows small biases in the fitted parameters (Table IV). A contribution to the systematic uncertainty is derived from these biases in Sec. IV D.

D. Systematic Uncertainties

Table V summarizes the systematic uncertainties for the measurement of the amplitudes. The sources of uncertainty we have considered are described here.

1. "c.m. energy": The center-of-mass energy, which defines the $m_{\rm ES}$ endpoint spectrum, enters as the parameter m_0 of the ARGUS function (Eq. (17)). The value (5.291 GeV/c^2) is changed by ± 2 MeV/c^2 (uncertainty on the beam energy in the

TABLE V: Systematic uncertainties in the relative phases (rad) and in the amplitude moduli squared, for the three K^* channels combined.

Source	$\delta_\parallel - \delta_0$	$\delta_\perp - \delta_0$	$|A_0|^2$	$|A_\parallel|^2$	$|A_\perp|^2$
1. c.m. energy	0.003	0.005	0.0018	0.0002	0.0016
2. Bkg. shape	0.002	0.003	0.0012	0.0001	0.0011
3. BR	0.000	0.001	0.0001	0.0001	0.0001
4. MC stat.	0.014	0.008	0.0027	0.0023	0.0024
5. Fit bias	0.036	0.025	0.0002	0.0022	0.0021
6. PID	0.005	0.004	0.0013	0.0023	0.0019
7. S wave	0.033	0.038	0.0029	0.0025	0.0005
Total	0.052	0.046	0.0048	0.0046	0.0042

c.m. frame) and the largest deviation from the nominal fit result is taken as the estimate of the systematic uncertainty.

2. "Backgrounds shape": The ARGUS function shape parameter ξ (Eq. (17)), fitted to the $m_{\rm ES}$ spectrum, is changed by ± 1 standard deviation and the largest deviation from the nominal fit result is taken as the estimate of the systematic uncertainty.

3. "BR": The relative branching fractions of neutral and charged B mesons to J/ψ K^* affects the amount of cross-feed. The branching ratios are changed independently by ± 1 standard deviation [34] and the largest difference is taken as the systematic uncertainty.

4. "MC stat.": The finite Monte Carlo sample size induces a limited knowledge of the coefficients Φ^b_k. This effect is evaluated by splitting the original Monte Carlo sample into ten equal-sized subsamples, each of which is used to compute the Φ^b_k coefficients. These coefficients are then used for ten angular fits on the data, all differences being thus due to differences of the Φ^b_k coefficients. For each fitted parameter, the standard deviation is computed, and divided by $\sqrt{10}$ to estimate the "MC stat." effect due to the original Monte Carlo finite size.

5. "Fit bias": Biases are observed in validation studies (Table IV). The observed bias is used as an estimate of the systematic uncertainty.

6. "PID": The efficiency of the particle identification has angular dependence. The induced effect on the fitted parameters is corrected by the acceptance-correction scheme. Imperfect knowledge of the particle-identification efficiency will result in a bias. A conservative estimate of the systematic uncertainty is obtained by using acceptance-correction factors for different beam conditions, corresponding to the years 2000, 2001, and 2002, and using

the largest differences as estimates of the systematic uncertainties.

7. "S wave": An additional fit is performed with the g_{S+P} PDF (see next Section). The full g_{S+P}-to-g_P shift is used as a conservative estimate of the contribution to the systematic uncertainty, as was done in Ref. [19].

E. Results of the Angular Analysis

Table VI summarizes the results of the fit to the angular distribution. The fitted values for each channel and for each year of data collection (with statistical uncertainties only) are shown. Keeping in mind the two-fold phase ambiguity (Eq. (4)), we obtain

$$
\begin{aligned}
\delta_\parallel - \delta_0 &= (2.73 \pm 0.10 \pm 0.05)\,\text{rad}, \\
\delta_\perp - \delta_0 &= (0.18 \pm 0.07 \pm 0.05)\,\text{rad}, \\
|A_0|^2 &= 0.566 \pm 0.012 \pm 0.005, \\
|A_\parallel|^2 &= 0.204 \pm 0.015 \pm 0.005, \\
|A_\perp|^2 &= 0.230 \pm 0.015 \pm 0.004,
\end{aligned}
\tag{27}
$$

where the correlation matrix of the fitted parameters $(\theta_A, \phi_A, \delta_\parallel - \delta_0, \delta_\perp - \delta_0)$ (Eq. (5)) is

$$
\begin{pmatrix}
1.00 & 0.00 & -0.04 & +0.04 \\
 & 1.00 & -0.23 & -0.09 \\
 & & 1.00 & +0.65 \\
 & & & 1.00
\end{pmatrix} .
$$

Angular distributions for the three channels are shown in Fig. 4. A forward-backward asymmetry is clearly visible in the comparison of the distributions of $\cos\theta_{K^*}$ for (pure P-wave) MC, generated with the amplitudes found in the data, and for the data samples themselves. This is due to S–P interference.

In a series of 168 simulated experiments of the same size as the data sample, we find that the probabilities for obtaining a larger likelihood than that observed for the data are 11%, 47%, 58%, and 25% for the $K^\pm\pi^\mp$, $K_S^0\pi^\pm$, $K^\pm\pi^0$, and combined samples, respectively.

The results for $J/\psi\ K^{*0}$ and $J/\psi\ K^{*\pm}$ decays are found to be compatible with each other (Table VI); this confirms the expectation of isospin symmetry.

From Eq. (27), we note that $\delta_\parallel - \delta_0$ differs from π by 3.6 standard deviations and that $\delta_\perp - \delta_0$ differs from 0 by 2.0 standard deviations. In order to determine the uncertainty in $\delta_\parallel - \delta_\perp$, the combined data sample is refit using $\delta_\parallel - \delta_\perp$ and $\delta_0 - \delta_\perp$ as phase parameters. The resulting amplitudes and the value of $\delta_0 - \delta_\perp$ were as before, and this refit yields

$$
\delta_\parallel - \delta_\perp = (\pi - (0.60 \pm 0.08 \pm 0.02))\,\text{rad}, \tag{28}
$$

where the systematic uncertainties have been estimated as in Sec. IV D. The $\delta_\parallel - \delta_\perp$ statistical uncertainty agrees
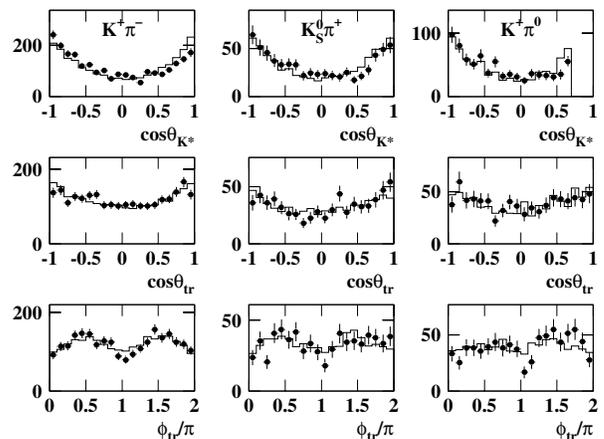

FIG. 4: Angular distributions. Histogram: Inclusive J/ψ MC sample ($p^*_{J/\psi} > 1.3$ GeV/c). Points: Data. The spectra are acceptance-corrected, background-subtracted, and normalized to the estimated yields (Table II). The visible forward-backward discrepancy in the $\cos\theta_{K^*}$ distribution is due to the $K\pi$ S-wave amplitude present in the data, and absent in the MC sample. The related systematic uncertainties in the measurements of the decay amplitudes are listed in line 7 of Table V.

with that expected from Eq. (27) taking into account the 65% correlation between the $\delta_\parallel - \delta_0$ and $\delta_\perp - \delta_0$ parameters. The departure from π is 7.6 standard deviations, and this demonstrates quite clearly the presence of final-state interactions between the J/ψ and the K^*.

V. RESOLVING THE STRONG PHASE AMBIGUITY

In our earlier publication [19] we presented evidence for the presence of a $K\pi$ S-wave amplitude in the $1.1 < m_{K\pi} < 1.3\,\text{GeV}/c^2$ range. We study this S wave in more detail here, in particular its interference with the P wave in the vicinity of the $K^*(892)$ resonance. We then use this interference to resolve the strong phase ambiguity for the $B \to J/\psi K^*(892)$ decay amplitudes, using the observations of Sec. I B.

In the following we will denote the two strong phase solutions obtained in the analysis of Sec. IV based on a purely P-wave angular distribution, by:

$$
\text{Solution I}: (\delta_\parallel - \delta_0, \delta_\perp - \delta_0) \simeq (2.7, 0.2), \tag{29}
$$
$$
\text{Solution II}: (\delta_\parallel - \delta_0, \delta_\perp - \delta_0) \simeq (-2.7, \pi - 0.2). \tag{30}
$$

The $K\pi$ mass requirement mentioned in Sec. III ($m_{K\pi}$ within 100 MeV/c^2 of the nominal $K^*(892)$ mass) is now relaxed, and the whole kinematical domain for the $K\pi$ system from $B \to J/\psi K\pi$ decay is used. The $m_{K\pi}$ spectra are shown in Fig. 5.

TABLE VI: Values of $|A_0|^2$, $|A_\parallel|^2$, $|A_\perp|^2$, $\delta_\parallel - \delta_0$, and $\delta_\perp - \delta_0$, for subsamples of the data divided according to decay channel. The first uncertainty is statistical; the second, when given, systematic. Note that the phases are subject to a two-fold ambiguity (Eq. (4)).

Sample	$|A_0|^2$	$|A_\parallel|^2$	$|A_\perp|^2$	$\delta_\parallel - \delta_0$ (rad)	$\delta_\perp - \delta_0$ (rad)
$K^\pm \pi^\mp$	$0.560 \pm 0.015 \pm 0.005$	$0.208 \pm 0.019 \pm 0.004$	$0.232 \pm 0.020 \pm 0.005$	$2.673 \pm 0.121 \pm 0.052$	$0.159 \pm 0.084 \pm 0.048$
$K_S^0 \pi^\pm$	$0.560 \pm 0.028 \pm 0.006$	$0.232 \pm 0.034 \pm 0.010$	$0.208 \pm 0.034 \pm 0.007$	$2.747 \pm 0.220 \pm 0.052$	$0.124 \pm 0.174 \pm 0.050$
$K^\pm \pi^0$	$0.592 \pm 0.028 \pm 0.013$	$0.165 \pm 0.032 \pm 0.011$	$0.243 \pm 0.036 \pm 0.009$	$2.904 \pm 0.287 \pm 0.090$	$0.329 \pm 0.176 \pm 0.066$
Total	$0.566 \pm 0.012 \pm 0.005$	$0.204 \pm 0.015 \pm 0.005$	$0.230 \pm 0.015 \pm 0.004$	$2.729 \pm 0.101 \pm 0.052$	$0.184 \pm 0.070 \pm 0.046$
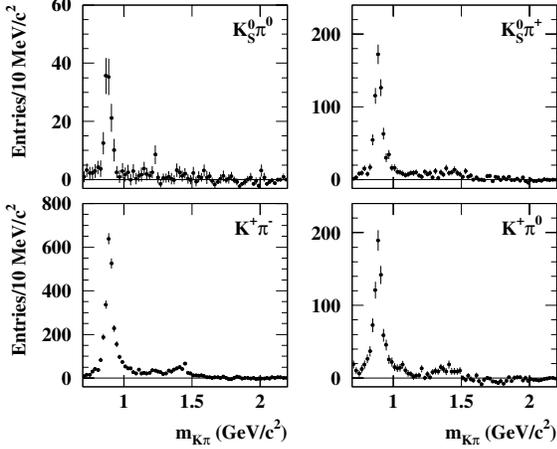
FIG. 5: The background-subtracted $K\pi$ invariant mass distributions for $J/\psi K\pi$ candidates in data.

A. Probing the S–P interference

We use the $K^\pm \pi^\mp$ sample since it is the largest sample and has the lowest background level. We split this sample into $K\pi$ mass intervals so that each interval has approximatly the same number of candidates. Equation (9) shows that the presence of both $K\pi$ P-wave and $K\pi$ S-wave amplitudes (i.e. $\lambda \neq 0$ and $\lambda \neq \pi/2$) implies the presence of S–P interference. Before fitting the data to the distribution of Eq. (9), we check for the presence of such interference effects by evaluating the moments of the angular functions $f_{8,9,10}$. The orthogonality of these functions is expressed by

$$
\int f_i(\boldsymbol{\omega}) f_j(\boldsymbol{\omega}) \mathrm{d}\boldsymbol{\omega} = \delta_{ij} \kappa_i \quad (i = 8, 9, 10 ;
$$

$$
j = 1, \ldots, 10), \quad (31)
$$

with $\kappa_8 = \kappa_9 = 3/40\pi$ and $\kappa_{10} = 3/4\pi$. The moments are defined by

$$
\langle f_i \rangle \equiv \int g_{S+P}(\boldsymbol{\omega}; m_{K\pi}, \boldsymbol{A}, \lambda) f_i(\boldsymbol{\omega}) \, \mathrm{d}\boldsymbol{\omega}, \quad (32)
$$

and are functions of $m_{K\pi}$. Using Eq. (32), we obtain for $i = 8, 9, 10$:

$$
\frac{2}{\kappa_8} \langle f_8 \rangle = \sin 2\lambda \cos(\delta_\parallel - \delta_S) |A_\parallel|,
$$

$$
\frac{2}{\kappa_9} \langle f_9 \rangle = \sin 2\lambda \sin(\delta_\perp - \delta_S) |A_\perp|,
$$

$$
\frac{2}{\kappa_{10}} \langle f_{10} \rangle = \sin 2\lambda \cos(\delta_S - \delta_0) |A_0|. \quad (33)
$$

The behaviour with $m_{K\pi}$ of the right side of Eq. (33) terms in data can be displayed by evaluating, in each $K\pi$ mass interval, the related moments. Their background-subtracted, acceptance-corrected distributions are shown in Fig. 6 for data. They show rapid variation near the position of the $K^*(892)$, where the phase of the P-wave changes most rapidly. Similar distributions obtained from inclusive J/ψ MC samples, in which no interference between S and P waves is simulated, show values of the moments compatible with zero in the corresponding mass range. In addition, the fact that the moments $\langle f_8 \rangle$, $\langle f_9 \rangle$, $\langle f_{10} \rangle$ show significant deviation from zero in the $K\pi$ mass region above 0.8 GeV/c^2 is a clear indication of the presence of an S-wave $K\pi$ amplitude in this region, interfering with the P-wave amplitudes.

We also note that the $\cos\theta_{K^*}$ forward-backward asymmetry

$$
A_{FB} \equiv \frac{N(\cos\theta_{K^*} > 0) - N(\cos\theta_{K^*} < 0)}{N(\cos\theta_{K^*} > 0) + N(\cos\theta_{K^*} < 0)}
$$

$$
= \frac{\sqrt{3}}{2} \sin 2\lambda \cos(\delta_S - \delta_0) |A_0| \quad (34)
$$

is proportional to $\langle f_{10} \rangle$ (Eq. (33)). The distribution of $\langle f_{10} \rangle$ (Fig. 6(c)) has a mean value of -0.14 ± 0.03 in the 0.8—1.0 GeV/c^2 $K\pi$ mass range, thus indicating a global $\cos\theta_{K^*}$ backward trend in the $K^*(892)$ region, as observed in Fig. 4.

B. Fitting for $\delta_S - \delta_0$

The $S + P$ angular distribution (Eq. (9)) is fit to the data in each $K\pi$ mass interval of Fig. 6 in order to obtain the values of λ and $\gamma = \delta_S - \delta_0$. Separate fits are performed for the two possible strong phase solutions (Eqs. (29,30)). We fix the P-wave amplitudes to
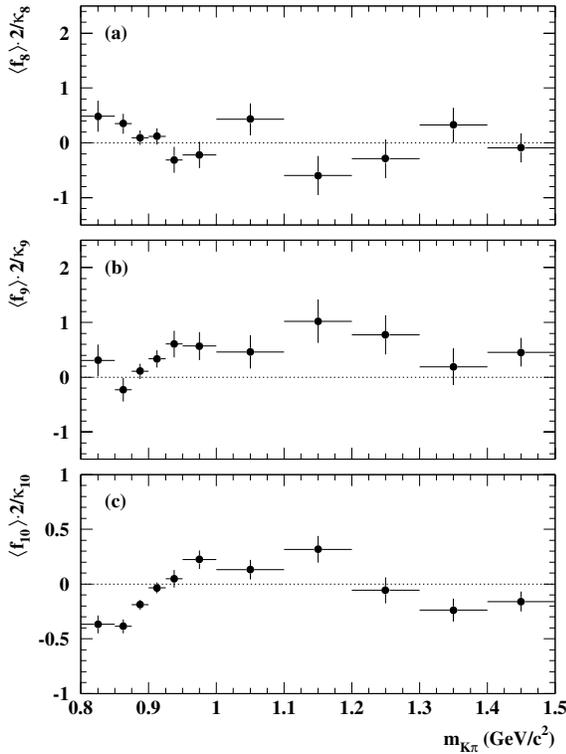
FIG. 6: Measured values of (a) $\langle f_8\rangle \cdot 2/\kappa_8$, (b) $\langle f_9\rangle \cdot 2/\kappa_9$ and (c) $\langle f_{10}\rangle \cdot 2/\kappa_{10}$, defined in Eq. (33), as a function of $m_{K\pi}$, for the $J/\psi\,K^\pm\pi^\mp$ candidates in data. The three distributions show a clear variation near the $K^*(892)$ region.
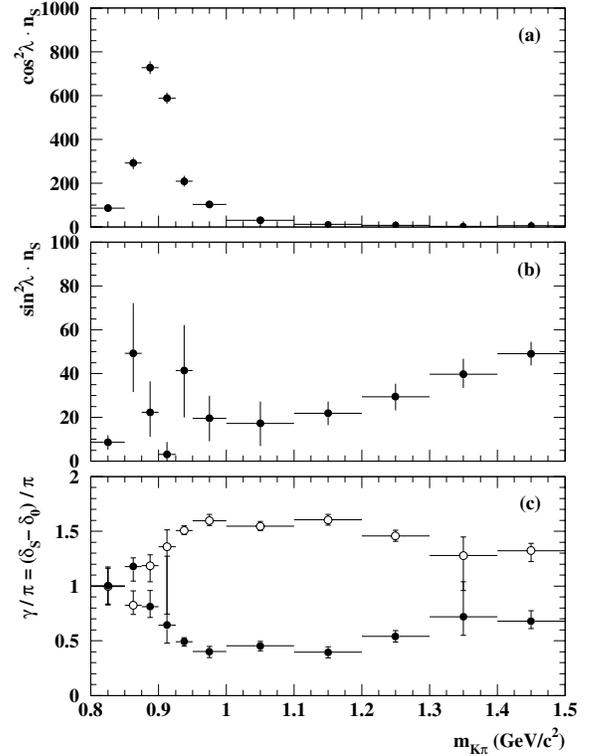

FIG. 7: (a) The P-wave intensity times number of events; i.e., $n_S\cos^2\lambda$; (b) the S-wave intensity times number of events; i.e., $n_S\sin^2\lambda$. These are the numbers of events that would be observed in each interval for the amplitude under consideration, if it were the only amplitude. The fraction of S-wave intensity integrated over the range $0.8 < m_{K\pi} < 1.0\,\mathrm{GeV}/c^2$ is found to be $(7.3 \pm 1.8)\%$. (c) The evolution of γ/π with $m_{K\pi}$, for the two sets of strong phases. The mirror symmetry described by Eq. (10) is clearly visible as $\gamma \leftrightarrow 2\pi - \gamma$. The error bars represent the statistical uncertainty in the fit of (λ, γ) in the $m_{K\pi}$ interval considered. All distributions are from fits to $J/\psi\,K^\pm\pi^\mp$ candidates in data.

the values obtained previously (Eq. (27)). The methods for acceptance correction and background subtraction described in Sec. IV are also applied here. Any variation of the acceptance with $m_{K\pi}$ is neglected.

The fit results for the $K^\pm\pi^\mp$ channel are shown in Fig. 7. Figure 7(a) shows the P-wave intensity, namely $\cos^2\lambda \cdot n_S$, and Fig. 7(b) shows the S-wave intensity. The quantity n_S is the estimated number of signal events in the given $m_{K\pi}$ mass interval and is obtained from a fit similar to that in Fig. 3, but with the Gaussian parameters fixed to the values obtained there.

Figure 7(c) shows the phase γ as a function of $m_{K\pi}$ for the two solutions for the strong phases (Eqs. (29,30)). We see that the two solutions show opposite behavior in each mass interval, as they must (see Eq. (10)). The large excursion in the relative phase in passing through the $K^*(892)$ region supports our assumption that the phases of the decay amplitudes reflect the phases of the simple $K\pi$ system.

The full points of Fig. 7(c) are obtained with strong phases of "Solution II", for which γ is decreasing in the $K^*(892)$ region, as required for the physical solution. A conservative estimate of the discrimination between the two solutions is made by fitting for the slope $d\gamma/dm_{K\pi}$ in the range $0.8 < m_{K\pi} < 1.0$ GeV/c^2; we find

$$
\begin{aligned}
\text{Solution I:} & \quad 16.2 \pm 2.7 \ \mathrm{rad/\,GeV}/c^2 \\
\text{Solution II:} & \quad -16.2 \pm 2.7 \ \mathrm{rad/\,GeV}/c^2
\end{aligned}
$$

As they must, these two slopes have opposite values. The two fits have a χ^2 per degree of freedom of 1.6. Finally, interpreting Solution II as the physical solution, we obtain the unique result

$$
\begin{aligned}
\delta_\parallel - \delta_0 &= (-2.73 \pm 0.10 \pm 0.05)\,\mathrm{rad}, \\
\delta_\perp - \delta_0 &= (+2.96 \pm 0.07 \pm 0.05)\,\mathrm{rad}, \quad (35)
\end{aligned}
$$

i.e., the two relative phase values are approximately equal in magnitude but with opposite sign.

It should be noted that this phase solution is not that selected in previous papers, nor in Eq. (27).

C. Examining the Moments

The values of the moments $\langle f_8 \rangle$, $\langle f_9 \rangle$, and $\langle f_{10} \rangle$ (Eq. (33)) are unchanged under the strong phases transformation Eq. (10), and, as such, do not allow us to distinguish between Solution I and II; but we show here that their variation, in particular that of $\langle f_9 \rangle$, with $m_{K\pi}$, together with the physical requirement that $d\gamma/dm_{K\pi} < 0$, allows us to resolve the ambiguity, without relying on the explicit solutions displayed in Fig. 7(c).

Since λ is small and positive, $\sin 2\lambda > 0$ and from Eq. (33) we can write

$$\frac{d\langle f_8 \rangle}{dm_{K\pi}} \sim + \sin(\delta_\parallel - \delta_0 - \gamma)\frac{d\gamma}{dm_{K\pi}}, \qquad (36)$$

$$\frac{d\langle f_9 \rangle}{dm_{K\pi}} \sim - \cos(\delta_\perp - \delta_0 - \gamma)\frac{d\gamma}{dm_{K\pi}}, \qquad (37)$$

$$\frac{d\langle f_{10} \rangle}{dm_{K\pi}} \sim - \sin\gamma \frac{d\gamma}{dm_{K\pi}}. \qquad (38)$$

Given that the values for $\delta_\parallel$ and $\delta_\perp$ are close to 0 or π (Eqs. (29,30)), we can approximate Eqs. (36,37) by

$$\frac{d\langle f_8 \rangle}{dm_{K\pi}} \sim - \cos(\delta_\parallel - \delta_0)\sin\gamma\frac{d\gamma}{dm_{K\pi}}, \qquad (39)$$

$$\frac{d\langle f_9 \rangle}{dm_{K\pi}} \sim - \cos(\delta_\perp - \delta_0)\cos\gamma\frac{d\gamma}{dm_{K\pi}}. \qquad (40)$$

On Fig. 6(c) we observe, in the $K^*(892)$ region, that

$$\langle f_{10} \rangle \sim + \cos\gamma \ < 0, \qquad (41)$$

$$\frac{d\langle f_{10} \rangle}{dm_{K\pi}} \sim - \sin\gamma\frac{d\gamma}{dm_{K\pi}} \ > 0, \qquad (42)$$

meaning that

$$\frac{d\langle f_8 \rangle}{dm_{K\pi}} \quad \text{has the sign of} \quad \cos(\delta_\parallel - \delta_0), \qquad (43)$$

$$\frac{d\langle f_9 \rangle}{dm_{K\pi}} \quad \text{has the sign of} \quad \cos(\delta_\perp - \delta_0)\frac{d\gamma}{dm_{K\pi}}. \qquad (44)$$

The variation of $\langle f_8 \rangle$ observed on Fig. 6(a) is compatible with Eq. (43), whichever strong phase solution is considered (Eqs. (29,30)) and thus cannot distinguish between the physical solution and the non-physical one. Figure 6(b) shows that $d\langle f_9 \rangle/dm_{K\pi} > 0$, meaning that either

$$\cos(\delta_\perp - \delta_0) > 0 \quad \text{and} \quad \frac{d\gamma}{dm_{K\pi}} > 0, \qquad (45)$$

$$\cos(\delta_\perp - \delta_0) < 0 \quad \text{and} \quad \frac{d\gamma}{dm_{K\pi}} < 0. \qquad (46)$$

We note that $\cos(\delta_\perp - \delta_0) > 0$ for Solution I (Eq. (29)), and $\cos(\delta_\perp - \delta_0) < 0$ for Solution II (Eq. (30)). The variation of $\langle f_9 \rangle$ with $m_{K\pi}$ provides thus the association of Solution II with the physical requirement $d\gamma/dm_{K\pi} < 0$, and of Solution I with the non-physical case $d\gamma/dm_{K\pi} > 0$. This leads to select Solution II as the physical solution, consistently with the previous section.
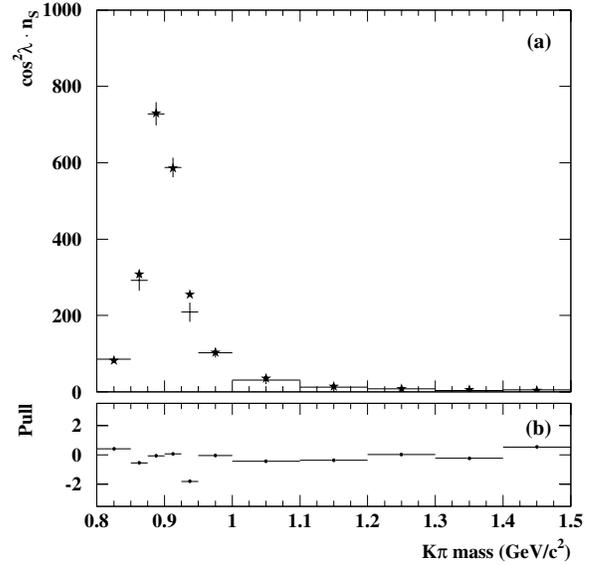

FIG. 8: (a) Comparison of the $K^\pm\pi^\mp$ P-wave intensity with a Breit-Wigner lineshape, including a centrifugal barrier factor, with world average parameters for $K^*(892)$ [34]. The lineshape is integrated in each mass interval (star markers) and compared with the measured intensity in that interval, after a minimun χ^2 fit of the overall normalization to the data in the 0.8–1.3 GeV/c^2 mass range. The χ^2 per degree of freedom is 0.86. (b) Pull (i.e. difference of measured and expected intensities, normalized to the uncertainty) in each mass interval.

D. Checking the $(K\pi)_{P-\text{wave}}$ lineshape

Figure 8 compares the P-wave intensity (as already shown in Fig. 7(a)) with a Breit-Wigner lineshape, including a centrifugal barrier factor, using the world average [34] parameter values for $K^*(892)$. (The mass resolution is about 3 MeV/c^2 and is negligible in its effect.) The overall normalization is fit in the 0.8–1.3 GeV/c^2 mass range. The χ^2 per degree of freedom is 0.86. The good agreement observed between the data and the Breit-Wigner lineshape suggests that the final-state interactions observed at the end of Sec. IV E, though statistically significant, are not so great as to distort the lineshape. This is consistent with our hypothesis of small interaction between the J/ψ meson and the $K\pi$ system, made at the end of Sec. I B.

E. Comparison with $K^- p \to K^- \pi^+(n)$ Scattering Results

In Fig. 9 we compare the evolution of γ observed in Fig. 7(c) with that obtained from the LASS measurement of $K^- p \to K^- \pi^+(n)$ scattering. The LASS points [39] (based on data from Refs. [22, 40]), represented as dia-

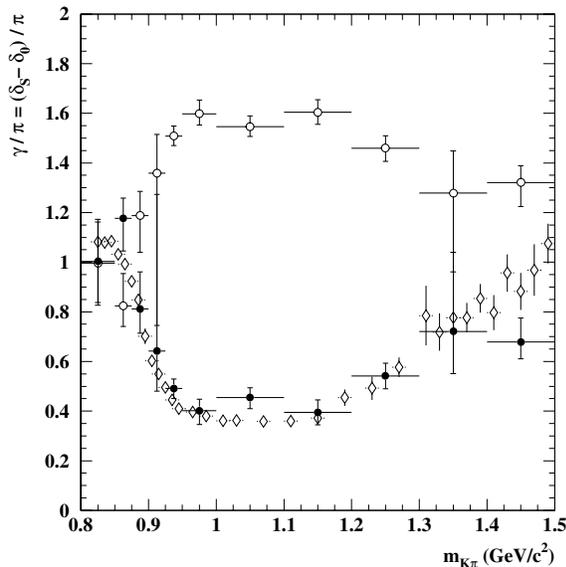FIG. 9: Comparison of the variation of $\gamma = \delta_S - \delta_0$ with $m_{K\pi}$ for the $J/\psi K^{\pm}\pi^{\mp}$ events, for "Solution I" (open points, Eq. (29)) and "Solution II" (full points, Eq. (30)), with that measured by the LASS experiment [22, 39, 40] (diamond markers).

monds, show the phase difference

$$\delta_{S(I=1/2)} - \delta_{P(I=1/2)}$$

as a function of $m_{K\pi}$. Only the $I = 1/2$ amplitude is retained since this is the only one produced by the $B \to J/\psi K\pi$ process. The LASS analysis takes into account the D wave, while the present analysis does not, but the D wave ($K_2^*(1430), \Gamma \sim 100$ MeV) has an effect only at high $m_{K\pi}$. An overall shift of π radian is added to the LASS phase difference measurements in order to match the sign of the forward-backward asymmetry observed with the $B \to J/\psi K\pi$ events. This shift does not modify the slope and general shape that are of interest here. The shift corresponds merely to changing the relative sign between the S and P wave amplitudes. The need for such a global shift is not surprising since the production processes are unrelated. We can see that the agreement between "Solution II" and LASS is striking (Fig. 9).

VI.   MEASUREMENT OF cos 2β

To measure cos2β, we perform an unbinned maximum likelihood fit to the differential decay rate as a function of proper time and the three angular variables (Eqs. (11,12)) for the $B^0 \to J/\psi K^{*0}(K_S^0\pi^0)$ sample. The amplitude parameters $|A_0|$, $|A_\perp|$, $|A_\parallel|$, $\delta_\parallel - \delta_0$, and $\delta_\perp - \delta_0$ in Eq. (12) are fixed to those obtained by the angular analysis of the three high-statistics flavor-specific $B \to J/\psi K^*$ channels, presented in Secs. IV and V. In

TABLE VII: Composition of the reconstructed $B^0 \to J/\psi K^{*0}(K_S^0\pi^0)$ candidate sample in the region $m_{ES} > 5.27$ GeV/c^2. The background fractions are estimated from an inclusive J/ψ Monte Carlo sample with an equivalent integrated luminosity of 590 fb^{-1} with the requirement $p_{J/\psi}^* > 1.3$ GeV/c. The first uncertainty is statistical; the second is systematic and is based on the uncertainty in the corresponding branching fraction [34] if it is known, and otherwise is based on a 50% uncertainty on the branching fraction used in the Monte Carlo generator.

	Fraction(%)	Effective CP
Signal	$83.0 \pm 1.2 \pm 5.7$	
Cross-feed	$3.2 \pm 0.5 \pm 0.3$	0
$B^0 \to \chi_{c1} K_S^0$	$4.0 \pm 0.6 \pm 1.1$	-1
Higher-mass K^* resonances	$3.5 \pm 0.6 \pm 1.8$	0 ± 1
Non-resonant $B^0 \to J/\psi K_S^0\pi^0$	$2.8 \pm 0.5 \pm 1.4$	0 ± 1
Other $B \to J/\psi X$	$3.5 \pm 0.6 \pm 1.8$	0 ± 1

particular, the strong phases $\delta_\parallel - \delta_0$ and $\delta_\perp - \delta_0$ are fixed to "Solution II" (Eq. (30,35)), described in Sec. V.

We examine each event with a $B^0 \to J/\psi K^{*0}(K_S^0\pi^0)$ candidate, indicated by B_{CP}, for evidence that the other neutral B meson, B_{tag}, decayed as a B^0 or a $\overline{B}^0$ (flavor tag, as described below). We also determine the decay proper-time difference $\Delta t \equiv t_{CP} - t_{tag}$, which corresponds to the variable t in Eqs. (11)-(15). To a good approximation $c \cdot \Delta t = \Delta z/(\gamma_B \cdot \beta \cdot \gamma)$ where Δz is the separation between the B_{CP} and B_{tag} vertices along the e^+e^- collision axis and $\gamma_B \cdot \beta \cdot \gamma = (p_{e^-} - p_{e^+})/(2 \cdot m_B)$.

The background level in the $B^0 \to J/\psi K_S^0\pi^0$ sample is higher than in the other $B \to J/\psi K\pi$ channels. In particular, some CP-violating backgrounds tend to peak in the signal region ($m_{ES} > 5.27$ GeV/c^2), making the $m_{ES} < 5.27$ GeV/c^2 region a poorer representation of the background behaviour than in the other $B \to J/\psi K\pi$ channels. In contrast with the method used for the angular analysis described above, the CP analysis is performed by the maximizing a likelihood function that contains the PDFs of both the signal and the background. Only events from the signal region are used. Monte Carlo samples are used to determine the angular acceptance, and the background composition and angular dependence, as described in the following Sections.

A.   Background Contributions

The inclusive J/ψ Monte Carlo sample is used to determine the composition of the $B^0 \to J/\psi K^{*0}(K_S^0\pi^0)$ candidate sample. The results are shown in Table VII. Aside from the signal and cross-feed contributions, the dominant contributions are from $B^0 \to \chi_{c1}K_S^0$ and $B^0 \to J/\psi K^{**}$ decays, where K^{**} denotes higher-mass K^* resonances. The angle- and Δt-dependent PDF for each of these backgrounds is described in the next Section.

B. Acceptance Description

The acceptance and the combinatorial background PDF are described by expansions in terms of products of spherical harmonics. The orthonormal basis functions used are

$$\mathcal{Y}_{LRM}(\boldsymbol{\omega}) \equiv \sqrt{2\pi} Y_{LM}(\theta_\psi, \chi) Y_{RM}(\theta_{K^*}, 0), \quad (47)$$

where θ_ψ, χ are the helicity angles corresponding to the transversity angles θ_{tr}, ϕ_{tr} [27] and the Y_{lm} are spherical harmonic functions. These $\mathcal{Y}_{LRM}$ functions describe the partial waves involved in a "Scalar $\rightarrow$ Vector X" decay, where X can be of arbitrary spin [14]. A function of $\boldsymbol{\omega}$, say $\epsilon(\boldsymbol{\omega})$, is expanded as:

$$\epsilon(\boldsymbol{\omega}) = \sum_{LRM} T^\epsilon_{LRM} \mathcal{Y}_{LRM}(\boldsymbol{\omega}), \quad (48)$$

where the sums over L and R run, in principle, from 0 to infinity, and the sum over M from $-\min(L, R)$ to $+\min(L, R)$.

The moments of the acceptance are estimated from Monte Carlo simulation, with N_{gen} events generated with PDF g, N_{obs} events being finally selected:

$$T^\epsilon_{LRM} \equiv \int \epsilon(\boldsymbol{\omega}) \mathcal{Y}^*_{LRM}(\boldsymbol{\omega}) d\boldsymbol{\omega}$$

$$\approx \frac{1}{N_{gen}} \sum_{i=1}^{N_{obs}} \frac{1}{g(\boldsymbol{\omega}_i)} \mathcal{Y}^*_{LRM}(\boldsymbol{\omega}_i). \quad (49)$$

The moments for the background PDFs are computed using the reconstructed events of the MC background sample distributed as $b(\boldsymbol{\omega})$:

$$T^b_{LRM} = \int b(\boldsymbol{\omega}) \mathcal{Y}^*_{LRM}(\boldsymbol{\omega}) d\boldsymbol{\omega}$$

$$\approx \frac{1}{N_b} \sum_{i=1}^{N_b} \mathcal{Y}^*_{LRM}(\boldsymbol{\omega}_i). \quad (50)$$

We note that the analytical expressions for the background PDF and for the efficiency are not needed to compute these moments. The expansion is done up to rank $L = R = 4$ for the acceptance (signal distribution is of rank 2) and up to rank $L = R = 6$ for the background. These ranks are chosen to be large enough so that no significant deviation of the fitted parameters $\sin 2\beta$ and $\cos 2\beta$ is observed in high-statistics Monte Carlo samples when compared to the generated values.

C. The B$_{flav}$ Sample

The fit is additionally performed on a large sample of fully reconstructed B^0 decays to flavor eigenstates (B_{flav}) with decays $B^0 \rightarrow D^{(*)\pm} h^\mp$, where $h = \pi, \rho, a_1$ and $B^0 \rightarrow J/\psi K^{*0}$ ($K^{*0} \rightarrow K^\pm \pi^\mp$). These events are

used to measure the parameters of the flavor-tagging algorithm and of the Δt-resolution functions. Flavor tagging performance is shown to be independent of the fully-reconstructed B meson and the Δt resolution is dominated by the vertex resolution of the incompletely reconstructed tagging B meson. Thus both tagging and Δt resolution can be studied with these large, well understood samples and the results applied to the channels of interest.

The fully reconstructed B meson, i.e., B_{flav} or B_{CP}, is denoted by B_{rec}.

D. Flavor Tag Determination

We use a multivariate technique [3] to determine the flavor of the B_{tag} meson. Separate neural networks are trained to identify primary leptons, kaons, soft pions from D^* decays, and high-momentum charged particles from B decays. Events are assigned to one of five mutually exclusive tagging categories based on the estimated mistag probability and the source of the tagging information: `Lepton`, `Kaon I`, `Kaon II`, `Inclusive` and `Untagged`. The `Untagged` events are not used in this analysis.

We determine the average dilution $\langle D \rangle$ and dilution difference ΔD, defined as

$$\overline{D} \equiv 1 - 2\overline{w},$$
$$D \equiv 1 - 2w,$$
$$\langle D \rangle \equiv \frac{D + \overline{D}}{2},$$
$$\Delta D \equiv D - \overline{D}, \quad (51)$$

for each tagging category, where w ($\overline{w}$) is the probability that a flavor tag determination is incorrect when the true tag is a B^0 ($\overline{B}^0$). The quality of the tagging is expressed in terms of the effective efficiency $Q \equiv \sum_k \epsilon_k (1 - 2w_k)^2$, where ϵ_k and w_k are the efficiencies and mistag probabilities, respectively, for events tagged in category k. The tagging performance is measured in a large data sample of fully reconstructed B decays. The effective tagging efficiency is $(28.1 \pm 0.7)\%$ [3]. The tagging efficiency asymmetry between B^0 and $\overline{B}^0$ has been studied [27, 41] using the full simulation of the experiment and has been found to be negligible for this analysis.

E. Determination of Δt and Δt Resolution

The proper-time difference Δt between the decays of the two B mesons in the event (B_{rec}, B_{tag}) is determined from the measured separation along the collision axis, Δz, between the B_{rec} and the B_{tag} vertices (Eq. (22) of Ref. [32].) The B_{tag} decay vertex is obtained by fitting tracks that do not belong to the B_{rec} candidate, imposing constraints from the B_{rec} momentum and the beam spot location. The average Δt resolution is approximately 1.1

ps. We require that the measured proper-time difference between the B_{rec} and the B_{tag} decays satisfies $|\Delta t| <$ 20 ps and that the estimated uncertainty in Δt, $\sigma_{\Delta t}$, which is derived from the vertex fit for the event, be less than 2.5 ps.

The Δt-resolution function $\mathcal{R}$ is represented by a sum of three Gaussian distributions (called the core, tail, and outlier components):

$$
\begin{aligned}
\mathcal{R}(\delta(\Delta t)) \equiv\ & f_{core}\mathrm{G}(\delta(\Delta t); \mu_{core}, \sigma_{core})\ + \\
& f_{tail}\mathrm{G}(\delta(\Delta t); \mu_{tail}, \sigma_{tail})\ + \\
& f_{outlier}\mathrm{G}(\delta(\Delta t); \mu_{outlier}, \sigma_{outlier}), \quad (52)
\end{aligned}
$$

where G is the Gaussian function, $\delta(\Delta t) \equiv \Delta t - \Delta t_{\mathrm{true}}$, Δt_{true} is the actual decay time difference, and f_{core}, f_{tail}, and $f_{outlier}$ the fractions of each component.

For the width of the core and tail Gaussians (σ_{core}, σ_{tail}), we use the measurement uncertainty $\sigma_{\Delta t}$ and allow separate scale factors S_{core} and S_{tail} to accommodate an overall underestimate ($S_k > 1$) or overestimate ($S_k < 1$) of the errors for all events, so that $\sigma_{core} = S_{core}\sigma_{\Delta t}$ and $\sigma_{tail} = S_{tail}\sigma_{\Delta t}$.

The core and tail Gaussian distributions are allowed to have a nonzero mean (μ_{core}, μ_{tail}) to account for charm decay products possibly included in the B_{tag} vertex. In the resolution function, these mean offsets are scaled by the event-by-event measurement error $\sigma_{\Delta t}$ to account for

an observed correlation [32] between the mean of the $\delta(\Delta t)$ distribution and the measurement error $\sigma_{\Delta t}$ in Monte Carlo simulation. For the core we allow different means for each flavor-tagging category. One common mean is used for the tail components. The third Gaussian has a fixed width $\sigma_{outlier} = 8\,\mathrm{ps}$ and no offset ($\mu_{outlier} = 0$); it accounts for fewer than 1% of events, typically due to incorrectly reconstructed vertices.

F. Likelihood Function

We maximize the log-likelihood given by

$$
L_{total} = L_{CP} + L_{flav}, \quad (53)
$$

$$
\begin{aligned}
L_{CP} =\ & \sum_{tag,c} \sum_{i=1}^{N_{obs}} \ln \Bigg[f_0 b_0 + f_\pm b_\pm \\
& + (1 - (f_0 + f_\pm))\, g^{K_S^0\pi^0,\ \mathrm{obs}} \Bigg], \quad (54)
\end{aligned}
$$

where f_0 and $f_\pm$ are the fractions of "neutral" and "charged" background in the CP sample, and b_0 and $b_\pm$ are the corresponding background PDFs, described below. The signal PDF $g^{K_S^0\pi^0,\ \mathrm{obs}}$ is

$$
\begin{aligned}
g_\zeta^{K_S^0\pi^0,\ \mathrm{obs}}(\boldsymbol{\omega}, \Delta t; \boldsymbol{A}, \sin 2\beta, \cos 2\beta)\ =\ & \epsilon(\boldsymbol{\omega})\frac{\Gamma_0}{2}\mathcal{A}(\boldsymbol{\omega}; \boldsymbol{A}) \times \\
& \left\{ \left[1 + \zeta\left(\frac{\Delta D}{2}\right)\right] e_{\mathcal{R}}(\Delta t) - \zeta\langle D\rangle \left[c_{\mathcal{R}}(\Delta t)\frac{\mathcal{P}(\boldsymbol{\omega}; \boldsymbol{A})}{\mathcal{A}(\boldsymbol{\omega}; \boldsymbol{A})} + s_{\mathcal{R}}(\Delta t)\left(\frac{\mathcal{S}(\boldsymbol{\omega}; \boldsymbol{A})}{\mathcal{A}(\boldsymbol{\omega}; \boldsymbol{A})}\sin 2\beta + \frac{\mathcal{C}(\boldsymbol{\omega}; \boldsymbol{A})}{\mathcal{A}(\boldsymbol{\omega}; \boldsymbol{A})}\cos 2\beta\right)\right] \right\} \\
& \Bigg/ \left\{ \left[1 + \zeta\frac{\Delta D}{2}\right] \sum_{k=1,2,3,5} \mathcal{A}_k \Phi_k - \zeta\langle D\rangle\frac{1}{1+x_d^2} \sum_{k=4,6} \mathcal{A}_k \Phi_k \right\}, \quad (55)
\end{aligned}
$$

where ζ labels the flavor of the tagging B meson ($\zeta = 1$) or $\overline{B}^0$ meson ($\zeta = -1$), and $x_d = \Delta m/\Gamma_0$. $\mathcal{A}_k$ is defined by Eq. (23), and Φ_k is the diagonal part of $\Phi_k^{b=K_S^0\pi^0}$ defined in Eq. (22). Only $\varepsilon^{b\to b}, b = K_S^0\pi^0$ (Eq. (22)) is considered because the cross-feed is treated separately here, in the background contribution, as it does not contribute to CP violation. The Δt-resolution function $\mathcal{R}$ (Eq. (52)) appears in the following convolutions:

$$
\begin{aligned}
e_{\mathcal{R}}(\Delta t) &\equiv e^{-\Gamma_0|\Delta t_{true}|} \otimes \mathcal{R}(\delta(\Delta t)), \\
s_{\mathcal{R}}(\Delta t) &\equiv e^{-\Gamma_0|\Delta t_{true}|} \sin(\Delta m \Delta t_{true}) \otimes \mathcal{R}(\delta(\Delta t)), \\
c_{\mathcal{R}}(\Delta t) &\equiv e^{-\Gamma_0|\Delta t_{true}|} \cos(\Delta m \Delta t_{true}) \otimes \mathcal{R}(\delta(\Delta t)).
\end{aligned}
\quad (56)
$$

Most of the background is due to inclusive decays of B mesons to J/ψ (see Table III). We account for backgrounds with the following PDF's:

- Backgrounds from neutral-B decays (see Table VII) are parametrized with a form analogous to the one that describes $J/\psi K_S^0$, but with an effective CP eigenvalue, η_{CP}, and angle dependence $b(\boldsymbol{\omega})$:

$$
\begin{aligned}
b_{0,\zeta}(\Delta t, \boldsymbol{\omega}; \sin 2\beta, \eta_{CP}) \equiv\ & \frac{\Gamma_0}{2}e^{-\Gamma_0|\Delta t|} \times \\
& \left[\left(1 + \zeta\frac{\Delta D}{2}\right) - \zeta\langle D\rangle\eta_{CP}\sin 2\beta\sin(\Delta m\Delta t)\right] b(\boldsymbol{\omega}).
\end{aligned}
\quad (57)
$$

For $B^0 \to \chi_{c1}K_S^0$ the angular dependence $b(\boldsymbol{\omega})$ is

estimated with the Monte Carlo, and parametrized using an expansion in $\mathcal{Y}^*_{LRM}$. For higher-mass K^* resonances, non-resonant $B^0 \to J/\psi\, K^0_S \pi^0$, and other $B \to J/\psi\, X$ sources, a flat angular dependence is used.

- Backgrounds from charged B decays (see Table VII) are dominantly due to cross-feed from $B^{\pm} \to J/\psi\, K^{*\pm}$. They have a Δt distribution characterized by the decay rate Γ_+. They are represented by

$$b_{\pm,\zeta}(\Delta t, \boldsymbol{\omega}) \;\equiv\; \frac{\Gamma_+}{2} e^{-\Gamma_+|\Delta t|} \left(1 + \zeta \frac{\Delta D}{2} \right) b_{\pm}(\boldsymbol{\omega}). \tag{58}$$

The B_{flav} sample, which is used to determine the tagging features, enters the log-likelihood through the L_{flav} term (Eq.(53)), which is based on PDFs for "mixed" and "unmixed" events as is appropriate for these neutral B decays. The background PDFs include a zero-lifetime contribution, a contribution with an effective lifetime, and a contribution with an effective lifetime and an oscillating factor. The signal PDFs are

$$h_{u,\zeta}(\Delta t) \;\propto\; \left[\left(1 + \zeta \frac{\Delta D}{2} \right) + u\langle D \rangle \cos(\Delta m \Delta t) \right], \tag{59}$$

where $u = 1$ and $u = -1$ for unmixed and mixed events, respectively. A complete description of the log-likelihood L_{flav} term is provided in Ref. [32] ($\ln \mathcal{L}_{\mathrm{mix}}$ term in Eq.(6) of Ref. [32]).

Finally the free parameters in the fit are (see Table XI)

- $\sin 2\beta$ and $\cos 2\beta$ (2),
- the parameters for the signal Δt-resolution function (8),
- the tagging parameters for signal (8),
- the parameters for the background B_{flav} Δt resolution function (3),
- the parameters describing the composition of the background PDF for the B_{flav} sample (13).

In total there are 34 parameters. We fix Γ_0 and Δm to their world average values [34].

G.   Validation

The fitting scheme has been validated using the full simulation and the large parametrized MC samples mentioned above. No statistically significant bias is observed (Table VIII).

As a further cross-check, the data samples for the $B^{\pm} \to J/\psi\, K^{*\pm}$, channels, which are not expected to

TABLE VIII: Validation on full MC simulation [inclusive J/ψ MC sample ($p^*_{J/\psi} > 1.3$ GeV/c) and B_{flav} samples] and large parametrized MC samples. The generated values of $\sin 2\beta$ and $\cos 2\beta$ are 0.700 and 0.714, respectively.

CP Sample		$\sin 2\beta$	$\cos 2\beta$
Full MC	(0.6 ab^{-1})	0.61 ± 0.16	0.20 ± 0.32
Parametrized MC	(16 ab^{-1})	0.709 ± 0.017	0.705 ± 0.036

show any sizeable CP violation in the SM, are examined. For these channels, the differential decay rate does not have a $\sin \Delta m \Delta t$ contribution, so that the coefficients analogous to $\sin 2\beta$ and $\cos 2\beta$ should vanish. No significant deviation this expectation is observed (Table IX).

TABLE IX: Fit results for the $B^{\pm} \to J/\psi\, K^{*\pm}$ data control samples.

Sample	$\sin 2\beta$	$\cos 2\beta$
$B^{\pm} \to J/\psi\,(K^0_S \pi^{\pm})$	0.21 ± 0.20	-0.21 ± 0.47
$B^{\pm} \to J/\psi\,(K^{\pm} \pi^0)$	0.20 ± 0.20	-0.26 ± 0.46

H.   Systematic Uncertainties

The contributions to the systematic uncertainty are summarized in Table X. Systematic uncertainties (a) – (j) and (q) – (t) are in common with the $\sin 2\beta$ analysis [32] and are estimated in the same way. Systematic uncertainties (k) – (p) are specific to this $J/\psi\,(K^0_S \pi^0)$ analysis and are elaborated in the following:

(k) The systematic uncertainty due to imperfect knowledge of the fractions and CP values of the background sources is obtained by varying the fractions (see Table VII) by one standard deviation, if the background is measured, or by 50% of the branching fraction used in the Monte Carlo otherwise. The effective CP values (see Table VII) of unmeasured background is set to -1 and then to $+1$ to evaluate the effect on the measured parameters.

(m) Backgrounds are assumed to have the same dilutions as the signal. To evaluate the related uncertainty, the dilutions obtained from the $B^{\pm}$ sample are used and the difference in the results is taken as the systematic uncertainty.

(n) Random sets of amplitude moduli and strong phases are generated, according to a multi-Gaussian distribution, based on the covariance matrix obtained in the fit for the amplitudes and

on the sytematic uncertainties in the amplitudes. These amplitudes are used in place of the nominal amplitudes to evaluate the variation in the CP parameters. This procedure incorporates the uncertainties in the S-wave amplitude as well.

(o) The limited size of the Monte Carlo sample induces an uncertainty in the moments used to determine the acceptance and the background distribution. This is evaluated by splitting the Monte Carlo into ten samples, leading to ten CP measurements, and taking as an estimate of the uncertainty the RMS divided by $\sqrt{10}$.

(p) A flat angular distribution has been assumed for some of the background components (Sec. VI F). We estimate the magnitude of the related bias by computing the background moments from low-m_{ES} events.

TABLE X: Summary of systematic and statistical uncertainties on $\sin 2\beta$ and $\cos 2\beta$.

Source	$\sin 2\beta$	$\cos 2\beta$
Signal Properties		
(a) Δt-resolution function	± 0.002	± 0.002
(b) signal dilution B_{CP} vs B_{flav}	± 0.012	± 0.013
(c) Gaussian model for *outliers*	± 0.001	± 0.000
(d) f_{tail} parameter	± 0.002	± 0.003
(e) resolution/tagging correlation	± 0.001	± 0.001
(f) SVT alignment	± 0.010	± 0.030
Background properties: B_{flav}		
(g) signal probability	± 0.001	± 0.001
(h) ARGUS m_0 parameter	± 0.002	± 0.010
(i) oscillating contribution	± 0.001	± 0.022
(j) δ_{peak} contribution	± 0.001	± 0.003
J/ψ $(K_S^0 \pi^0)$ specific		
(k) background fraction and CP parity	± 0.032	± 0.142
(m) background dilutions	± 0.002	± 0.006
(n) amplitude uncertainties	± 0.016	± 0.154
(o) statistics used for moments	± 0.030	± 0.030
(p) angular background distribution	± 0.024	± 0.064
External parameters		
(q) z scale and "*boost*"	± 0.001	± 0.001
(r) beam spot	± 0.010	± 0.040
(s) B^0 lifetime	± 0.014	± 0.040
(t) Δm	± 0.018	± 0.032
Monte Carlo		
(u) Monte Carlo statistics	± 0.130	± 0.140
Total systematic uncertainty	± 0.14	± 0.27
Statistical uncertainty	± 0.57	$^{+0.76}_{-0.96}$

I. Results

The results of the fit are given in Table XI. Figure 10 shows the contour plots in the $\cos 2\beta$, $\sin 2\beta$ plane. We

obtain

$$\cos 2\beta \ = \ +3.32 \ ^{+0.76}_{-0.96}(\text{stat}) \pm 0.27(\text{syst}),$$
$$\sin 2\beta \ = \ -0.10 \pm 0.57(\text{stat}) \pm 0.14(\text{syst}). \quad (60)$$

The quality of the fit is estimated by generating 2000 experiments using the parametrized MC, and with the same sample size that is observed for the data. The probability to obtain a likelihood lower than that obtained from the data is found to be $(22 \pm 1)\%$.

When $\sin 2\beta$ is fixed to the value measured in B decays to $J/\psi K_S^0$ and related modes, $\sin 2\beta = \sin 2\beta_0 \equiv 0.731$ [4], we find

$$\cos 2\beta = +2.72^{+0.50}_{-0.79}(\text{stat}) \pm 0.27(\text{syst}). \quad (61)$$

J. Graphical Representation

The distribution of the time difference Δt is shown in Figs. 11(a) and 11(b), and the time-dependent asymmetry is shown in Fig. 11(c). Note that in the case of perfect acceptance this asymmetry is not sensitive to $\cos 2\beta$ [27].

A graphical representation of the sensitivity of the data to $\cos 2\beta$ is obtained from the time dependence of the moment of $\mathcal{C}$. Since $\mathcal{C}$ is orthogonal to both $\mathcal{A}$ and $\mathcal{S}$, we obtain, using Eq. (13)

$$\langle \mathcal{C} \rangle_\pm (\Delta t) \ \equiv \ \int g_\pm(\boldsymbol{\omega}, \Delta t; \boldsymbol{A}, \sin 2\beta, \cos 2\beta) \mathcal{C}(\boldsymbol{\omega}; \boldsymbol{A}) \, \mathrm{d}\boldsymbol{\omega}$$
$$= \ \pm \frac{\Gamma_0}{2} e^{-\Gamma_0 |\Delta t|} \times$$
$$\left\{ \cos(\Delta m \Delta t) \int \mathcal{P}(\boldsymbol{\omega}; \boldsymbol{A}) \mathcal{C}(\boldsymbol{\omega}; \boldsymbol{A}) \, \mathrm{d}\boldsymbol{\omega} \ + \right.$$
$$\left. \sin(\Delta m \Delta t) \cos 2\beta \int \mathcal{C}^2(\boldsymbol{\omega}; \boldsymbol{A}) \, \mathrm{d}\boldsymbol{\omega} \right\}.$$
$$(62)$$

We see that the magnitude of the $\sin(\Delta m \Delta t)$ oscillation is proportional to $\cos 2\beta$. The introduction of the angular acceptance $\epsilon(\boldsymbol{\omega})$ in principle breaks the above orthogonality, causing $\int \mathcal{AC}\epsilon \mathrm{d}\boldsymbol{\omega}$ and $\int \mathcal{SC}\epsilon \mathrm{d}\boldsymbol{\omega}$ terms to appear in the $\langle \mathcal{C} \rangle_\pm (\Delta t)$ expression, in addition to the $\int \mathcal{PC}\epsilon \mathrm{d}\boldsymbol{\omega}$ and $\int \mathcal{C}^2 \epsilon \mathrm{d}\boldsymbol{\omega}$ terms. These quantities are estimated using Monte Carlo and are found to be at the percent level of $\int \mathcal{C}^2 \epsilon \mathrm{d}\boldsymbol{\omega}$ for $\int \mathcal{AC}\epsilon \mathrm{d}\boldsymbol{\omega}$ and $\int \mathcal{SC}\epsilon \mathrm{d}\boldsymbol{\omega}$, and 14% of $\int \mathcal{C}^2 \epsilon \mathrm{d}\boldsymbol{\omega}$ for $\int \mathcal{PC}\epsilon \mathrm{d}\boldsymbol{\omega}$.

Figure 12 shows the moment of $\mathcal{C}$ as a function of Δt, overlaid with a function obtained from Eq. (62) that takes the acceptance into account.

K. Confidence Level for Positive $\cos 2\beta$ Solution

The value $\sin 2\beta = 0.731 \pm 0.056$ [4] measured in the charmonium-K^0 channel is in good agreement with expectations from the measurements of the sides of the Unitarity Triangle if the choice $\beta \approx 0.41 \equiv \beta_0$ is made. However, the alternative solutions $\beta \approx \pi/2 - 0.41, 0.41 + \pi,$

TABLE XI: Global CP fit of the $J/\psi\ K^{*0}$ ($K_S^0\ \pi^0$) events together with the B_{flav} sample. The transversity amplitudes used are those measured in the angular analysis. The $\cos2\beta$ value shown is the one corresponding to "Solution II" for the strong phases. The b's are the coefficients of the linear dependence of the Δt off-set on Δt uncertainty : $\langle\Delta t\rangle = b \times \sigma_{\Delta t}$.

Parameter	Value	Correlation with $\sin 2\beta$	Correlation with $\cos 2\beta$
$\sin 2\beta$	-0.10 ± 0.57	$+1.000$	-0.368
$\cos 2\beta$	$3.32^{+0.76}_{-0.96}$	-0.368	$+1.000$
Signal resolution function			
S_{core}	1.093 ± 0.048	-0.020	$+0.028$
S_{tail}	3.0 (fixed)		
b_{core} Lepton	0.012 ± 0.063	$+0.017$	-0.010
b_{core} Kaon I	-0.226 ± 0.052	$+0.008$	-0.050
b_{core} Kaon II	-0.248 ± 0.046	$+0.013$	-0.023
b_{core} Inclusive	-0.212 ± 0.047	$+0.020$	-0.020
b_{tail}	$-1.01\ \pm 0.29$	-0.021	$+0.029$
f_{tail}	0.109 ± 0.020	$+0.022$	-0.030
f_{out}	0.002 ± 0.001	-0.004	$+0.006$
Signal dilutions			
$\langle D\rangle$, Lepton	0.933 ± 0.013	-0.002	-0.004
$\langle D\rangle$, Kaon I	0.799 ± 0.014	-0.009	$+0.051$
$\langle D\rangle$, Kaon II	0.582 ± 0.016	-0.001	-0.006
$\langle D\rangle$, Inclusive	0.368 ± 0.017	$+0.009$	$+0.024$
ΔD, Lepton	0.031 ± 0.022	-0.003	-0.001
ΔD, Kaon I	0.023 ± 0.022	-0.010	$+0.039$
ΔD, Kaon II	0.090 ± 0.024	-0.008	$+0.002$
ΔD, Inclusive	0.050 ± 0.026	$+0.002$	$+0.004$
Background properties (B_{flav})			
τ [ps]	1.335 ± 0.064	$+0.001$	$+0.000$
$f(\tau=0)$ Lepton	$0.29\ \pm 0.17$	$+0.000$	-0.001
$f(\tau=0)$ Kaon I	0.631 ± 0.027	$+0.000$	-0.001
$f(\tau=0)$ Kaon II	0.659 ± 0.024	$+0.000$	-0.001
$f(\tau=0)$ Inclusive	0.684 ± 0.023	$+0.000$	$+0.000$
Background resolution function			
S_{core}	1.398 ± 0.019	$+0.001$	-0.002
b_{core}	-0.043 ± 0.013	-0.001	$+0.002$
f_{out}	0.015 ± 0.002	$+0.000$	$+0.001$
Background dilutions			
$\langle D\rangle$, Lepton , $\tau=0$	$1.36\ \pm 0.69$	$+0.000$	$+0.001$
$\langle D\rangle$, Kaon I , $\tau=0$	0.648 ± 0.030	$+0.001$	-0.004
$\langle D\rangle$, Kaon II , $\tau=0$	0.393 ± 0.023	$+0.000$	$+0.000$
$\langle D\rangle$, Inclusive , $\tau=0$	0.158 ± 0.024	-0.001	-0.002
$\langle D\rangle$, Lepton , $\tau>0$	$0.17\ \pm 0.11$	$+0.000$	$+0.000$
$\langle D\rangle$, Kaon I , $\tau>0$	0.251 ± 0.048	$+0.000$	$+0.000$
$\langle D\rangle$, Kaon II , $\tau>0$	0.278 ± 0.042	$+0.000$	$+0.000$
$\langle D\rangle$, Inclusive , $\tau>0$	0.031 ± 0.046	$+0.000$	$+0.000$

and $3\pi/2 - 0.41$ could turn out to be correct if there is a significant contribution from outside the Standard Model. We show here that we can exclude at a significant level of confidence the possibilities $\pi/2 - 0.41$ and $3\pi/2 - 0.41$, assuming that the value of $\sin2\beta$ that would be inferred from a high-statistics measurement of the $J/\psi K^*$ channel would conform to the measurement of Ref. [4]. We therefore constrain $\sin2\beta$ to $\sin2\beta_0$. The systematic uncertainty on β, induced by the uncertainty in $\sin2\beta$, (±0.056) [4] is ±0.043, which is negligible here.

We define $\cos2\beta_0 \equiv +\sqrt{1 - \sin^2 2\beta_0} \approx +0.68$. In the following, we estimate the confidence level at which the

$-\cos2\beta_0$ hypothesis can be excluded against the $+\cos2\beta_0$ solution.

1. Assuming Gaussian Statistics

Figure 13 shows the variation of the likelihood as a function of $\cos2\beta$. In the case of fixed $\sin2\beta$, the optimum is obtained at $\cos2\beta = +2.72$, 2.2σ from $+\cos2\beta_0$ and 3.5σ from $-\cos2\beta_0$. For a Gaussian distribution, the probabilities to observe values 2.2 and 3.5 σ from the mean value are, respectively, 3.25% and 0.08%. In
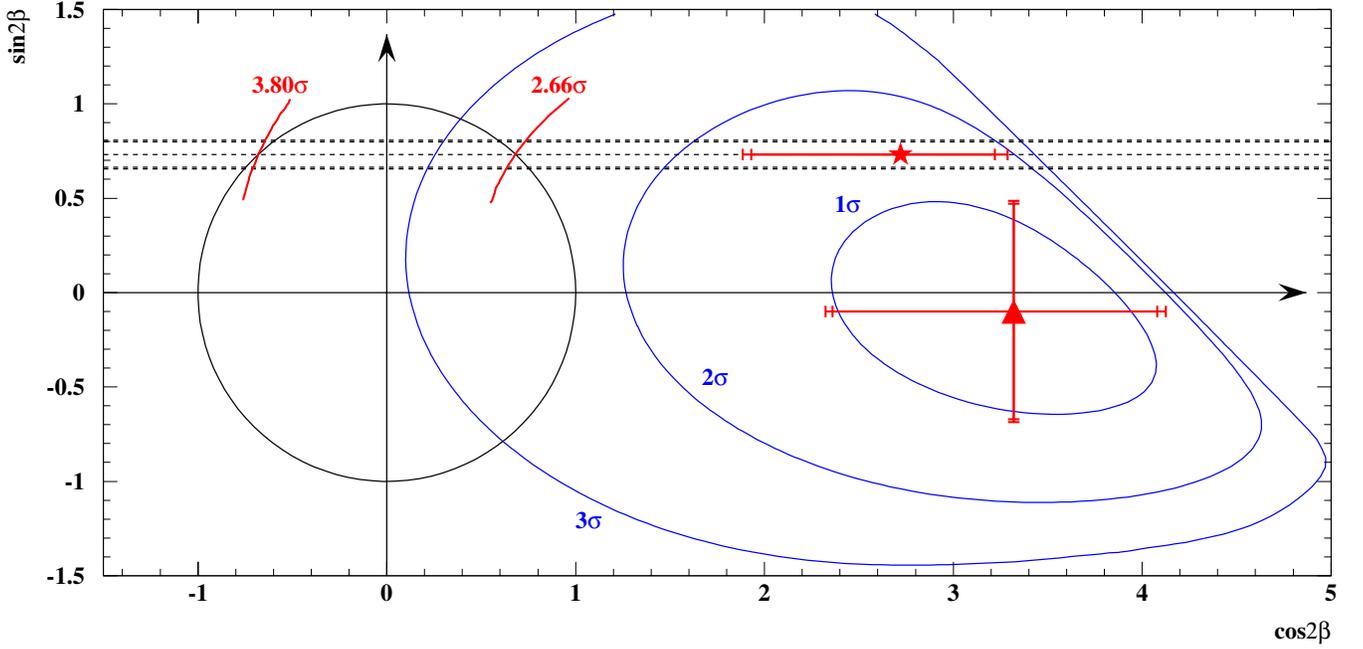
FIG. 10: Contour plots in the $\cos2\beta$, $\sin2\beta$ plane. The triangle denotes the result of the fit. The error bars show the statistical uncertainty and the quadratic sum of the statistical and systematic uncertainties. The star denotes the result of the fit with $\sin2\beta$ fixed at $\sin2\beta = 0.731$ [4]. The value of $\sin2\beta$ of reference [4] and its uncertainties are represented as dashed horizontal lines. The $n\sigma$ ($n = 1, 2, 3$) contour corresponds to a decrease of $0.5n^2$ in the log-likelihood with respect to the maximum value. The unit circle ($\cos^2 2\beta + \sin^2 2\beta = 1$) on which the true values must lie is also shown.

a Bayesian approach, assuming equal *a priori* probabilities for the $\pm\cos2\beta_0$ hypotheses, the probability that the $+\cos2\beta_0$ choice is wrong would be $0.08/(3.25 + 0.08) = 2.4\%$.

2. Using the Distribution of $\cos2\beta$ Values Obtained from Simulated Experiments

To take into account the nonparabolic shape of the log-likelihood as a function of $\cos2\beta$, $\cos2\beta$ values are measured with 2000 simulated samples, each the same size as the data sample (104 events) (Fig. 14). For the $+\cos2\beta_0$ hypothesis, the distribution $\frac{dN^+}{d\cos2\beta}$ of $\cos2\beta$ values is that shown in Fig. 14(c). An unbinned likelihood fit is performed to the sample of the 2000 $\cos2\beta$ values, with a sum of two Gaussian functions, $h(\cos2\beta)$. The fit result is shown in Fig. 15(a) (where $h(\cos2\beta)$ is scaled by 100, i.e., 2000 times the bin size).

The distribution $\frac{dN^-}{d\cos2\beta}$ is obtained by the transformation $\cos2\beta \rightarrow -\cos2\beta$: i.e., we have

$$\frac{dN^+}{d\cos2\beta}(\cos2\beta) = \frac{dN^-}{d\cos2\beta}(-\cos2\beta).$$

In a frequentist approach, we consider the probability that a result would disfavor, by at least as much as ours, the $-\cos2\beta_0$ hypothesis against the $+\cos2\beta_0$

one, by computing the probability to observe a ratio $r(\cos2\beta) \equiv \frac{dN^-}{d\cos2\beta}(\cos2\beta)/\frac{dN^+}{d\cos2\beta}(\cos2\beta)$ smaller than or equal to the one we obtain, $r(+2.72)$ [42]. Because this ratio $r(\cos2\beta)$ has a monotonic decreasing behaviour with $\cos2\beta$, the probability to obtain $r(\cos2\beta) \leq r(+2.72)$, if the true $\cos2\beta$ value is indeed $-\cos2\beta_0$, is

$$\begin{aligned} \alpha &\equiv \int_{+2.72}^{+\infty} \frac{dN^-}{d\cos2\beta}(\cos2\beta)\,d\cos2\beta \\ &= 0.6\%, \end{aligned} \tag{63}$$

leading to the confidence level at which the $-\cos2\beta_0$ hypothesis is excluded:

$$\begin{aligned} CL^{\text{Freq.}}(-\cos2\beta_0 \text{ excluded}) &\equiv 1 - \alpha \\ &= 99.4\%. \end{aligned} \tag{64}$$

If we ask how likely it is to obtain a result in the above $(+2.72, +\infty)$ range, if the true value of $\cos2\beta$ is $+\cos2\beta_0$, we find:

$$\int_{+2.72}^{+\infty} \frac{dN^+}{d\cos2\beta}(\cos2\beta)\,d\cos2\beta = 5.7\%. \tag{65}$$

In a frequentist interpretation, a high value for this last quantity would have indicated, together with the high $CL^{\text{Freq.}}(-\cos2\beta_0$ excluded) value obtained, that the $(+2.72, +\infty)$ domain would have allowed a sharp distinction between the two $\pm\cos2\beta$ hypotheses. The
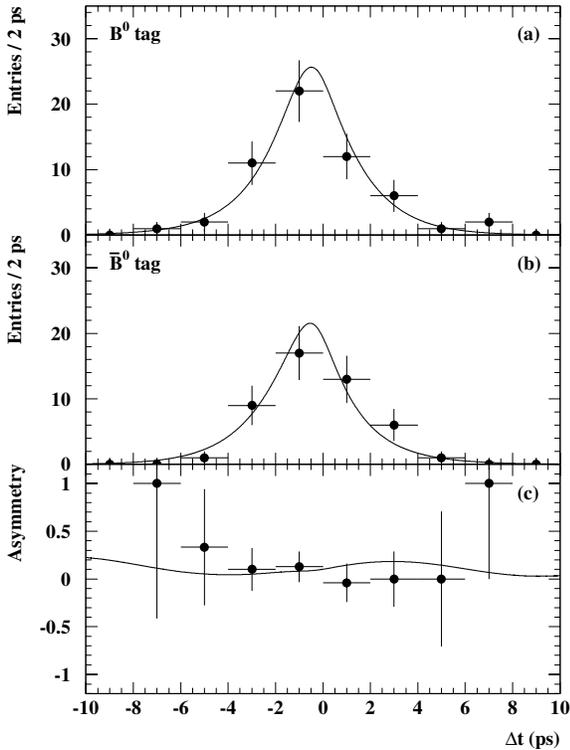
FIG. 11: The distribution of Δt for events in the signal region, for (a) B^0 and (b) $\overline{B}^0$ tags with the fit result (full curve) overlaid. In (c) we show the raw asymmetry in the number of B^0 and $\overline{B}^0$ tags in the signal region, $(N_{B^0} - N_{\overline{B}^0})/(N_{B^0} + N_{\overline{B}^0})$, for data, with the fit result (full curve) overlaid. Note that above distributions are not sensitive to $\cos 2\beta$ since this dependence vanishes when integrated over the angular variables.

rather low value observed here (5.7%) expresses that, at the present level of statistics, the discrimination between the $\pm \cos 2\beta_0$ hypotheses is rather modest. We can conclude however that our result would be somewhat more improbable (0.6%) if the true value of $\cos 2\beta$ were $- \cos 2\beta_0$ than it would be (5.7%) if the true value were $+ \cos 2\beta_0$.

In a Bayesian approach, assuming that the two $\pm \cos 2\beta_0$ hypotheses have *a priori* equal probabilities, the confidence level at which the $- \cos 2\beta_0$ solution is excluded, $CL(- \cos 2\beta_0 \text{ excluded})$, is obtained from $\frac{dN^+}{d\cos 2\beta}(+2.72)$ and $\frac{dN^-}{d\cos 2\beta}(+2.72)$ as follows:

$$
\begin{aligned}
CL(- \cos 2\beta_0 \text{ excluded}) &= \frac{h(+2.72)}{h(+2.72) + h(-2.72)} \\
&= \frac{6.64 \pm 0.38}{(6.64 \pm 0.38) + (0.86 \pm 0.15)} \\
&= (88.6 \pm 2.0)\%. \qquad (66)
\end{aligned}
$$

The probability to select incorrectly the $+ \cos 2\beta_0$ solution is significantly larger than for the previous Bayesian estimate based on Gaussian statistics (Sec. VI K 1).
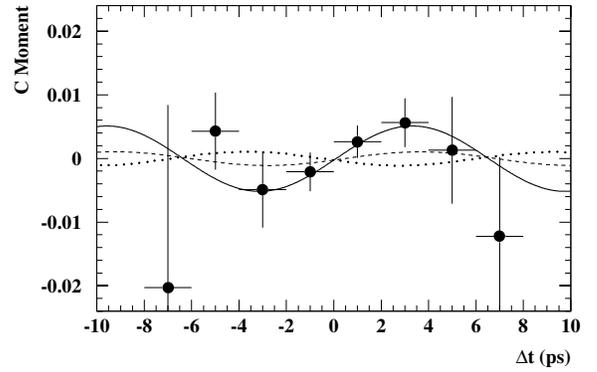
FIG. 12: The moment of $\mathcal{C}$ as a function of Δt. The overlaid curve corresponds to the fit results (Table XI). The dashed curve corresponds to $\cos 2\beta = +\sqrt{1 - \sin^2 2\beta_0} = +0.68$ [4], the dotted one to the non-standard solution $\cos 2\beta = -0.68$.
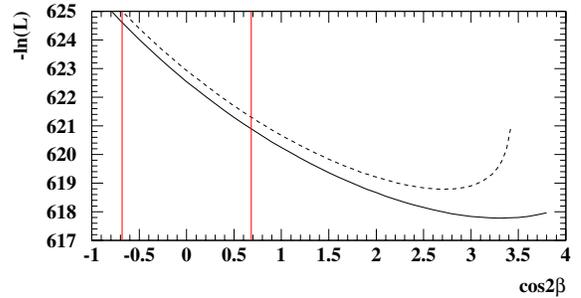
FIG. 13: The negative logarithm of the likelihood as a function of $\cos 2\beta$. Continuous line: $\sin 2\beta$ is a free parameter. Dashed line: $\sin 2\beta$ is fixed at $\sin 2\beta_0 = 0.731$ [4].

The uncertainty in Eq. (66) comes from the statistical uncertainties on $h(+2.72)$, $h(-2.72)$ (limited by the 2000 simulated experiments used), and their correlation (-6%). The systematic effects on the $\cos 2\beta$ measurement contribute to a $\pm 0.4\%$ variation of $CL(- \cos 2\beta_0 \text{ excluded})$ and are included in quadrature in the above uncertainty. We include a -1σ safety margin on $CL(- \cos 2\beta_0 \text{ excluded})$, and thus report

$$
CL(- \cos 2\beta_0 \text{ excluded}) = 86.6\%. \qquad (67)
$$

VII. CONCLUSION

We measure the transversity amplitudes of the decay to flavor eigenstates, $B \rightarrow J/\psi K^{*0}(K^\pm \pi^\mp)$ and $B \rightarrow J/\psi K^{*\pm}$ ($K^\pm \pi^0$ and $K_S^0 \pi^\pm$), with improved precision with respect to existing measurements. We deter-
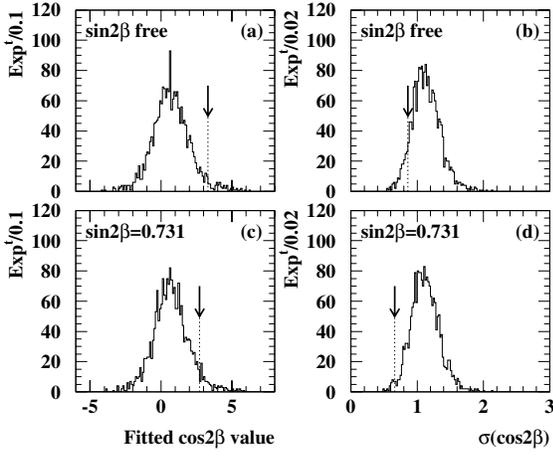
FIG. 14: The distribution of the values of $\cos 2\beta$ ((a) and (c)), and of the statistical uncertainties ((b) and (d)), obtained in 2000 simulated experiments, each based on a sample of the same size as the data; i.e., 104 events. These are taken from the parametrized MC sample mentioned above, with the generated $\cos 2\beta$ value $+0.68$. In (a) and (b) $\sin 2\beta$ is also free in the fit. In (c) and (d), $\sin 2\beta$ is fixed to the world average. The vertical arrows show the positions of the values obtained from the data.

mine

$$\delta_\parallel - \delta_0 = (-2.73 \pm 0.10 \pm 0.05)\,\text{rad},$$
$$\delta_\perp - \delta_0 = (+2.96 \pm 0.07 \pm 0.05)\,\text{rad},$$
$$|A_0|^2 = 0.566 \pm 0.012 \pm 0.005,$$
$$|A_\parallel|^2 = 0.204 \pm 0.015 \pm 0.005,$$
$$|A_\perp|^2 = 0.230 \pm 0.015 \pm 0.004, \tag{68}$$

and

$$\delta_\parallel - \delta_\perp = (0.60 \pm 0.08 \pm 0.02)\,\text{rad}. \tag{69}$$

We observe the presence of a significant S-wave amplitude interfering with the P-wave amplitude in the region of the $K^*(892)$. Using a novel method based on the dependence on the $K\pi$ invariant mass of the interference between the S- and P-waves, we resolve the ambiguity in the determination of the strong phases involved in B decays to $J/\psi K^*(892)$.

The values obtained for $|A_\parallel|^2$ and $|A_\perp|^2$ are consistent with being equal. The additional unambiguous determination of the phases relative to that of A_0 indicates that they have similar size but opposite sign, with a difference, $\delta_\parallel - \delta_\perp$, of 34 ± 5 degrees. Using the relations between the helicity amplitudes and the transversity amplitudes,

$$H_{+1} \equiv (A_\parallel + A_\perp)/\sqrt{2}$$
$$\equiv |H_+|e^{i\delta_+},$$
$$H_{-1} \equiv (A_\parallel - A_\perp)/\sqrt{2}$$
$$\equiv |H_-|e^{i\delta_-},$$
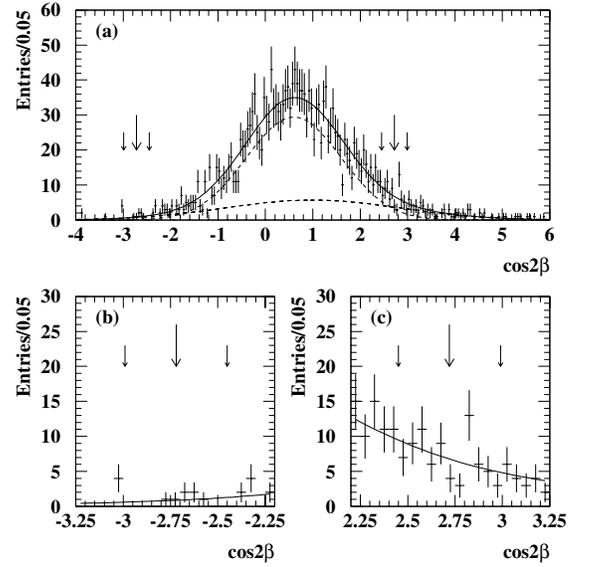$$H_0 \equiv A_0, \tag{70}$$

FIG. 15: (a) The $\cos 2\beta$ distribution for 2000 simulated experiments of the same size as the data sample, where the generated values for $\sin 2\beta$ and $\cos 2\beta$ are $+0.731$ and $+0.68$, respectively (same as Fig. 14(c)). An unbinned likelihood fit is performed to this distribution, using the sum of two Gaussian functions. The fit result is shown on the plot (full line) with the individual Gaussian contributions (dashed lines). The long vertical arrows show the $\cos 2\beta$ values ± 2.72. The small arrows indicate the extent of systematic uncertainties. (b) and (c) zoom on the $\cos 2\beta = \pm 2.72$ regions of Fig. 15(a). The densities of points at $+2.72$ and -2.72 are used to discriminate between the $\cos 2\beta = \pm\sqrt{1 - \sin^2 2\beta_0} = \pm 0.68$ hypotheses, as explained in the text.

TABLE XII: Helicity-amplitude moduli and phases for H_+ and H_- obtained from the measured transversity amplitudes (Eq. (68)) using Eq. (70). The corresponding configuration is shown in Fig. 16. The uncertainties are statistical only.

$|H_+|^2$	$|H_-|^2$	δ_+ (rad)	δ_- (rad)
0.396 ± 0.015	0.0379 ± 0.009	-3.04 ± 0.08	-1.36 ± 0.12

we obtain the moduli and phases given in Table XII. This determines the hierarchy of the helicity amplitudes in the decay to be $|H_0| : |H_{+1}| : |H_{-1}| \sim 0.75 : 0.63 : 0.19$. The corresponding configurations of the helicity and transversity amplitudes in the complex plane are illustrated in Fig. 16.

We confirm the presence of nonzero relative strong phases, with the difference between the phases of A_0 and $A_\parallel$ deviating from π with a significance of 3.6σ, and the phase difference between the two transverse amplitudes being 7.6σ from zero.

Treating $\sin 2\beta$ and $\cos 2\beta$ as independent quantities in the fit to the data, we obtain $\cos 2\beta = +3.32\,^{+0.76}_{-0.96}((\text{stat})) \pm 0.27((\text{syst}))$. When $\sin 2\beta$ is fixed
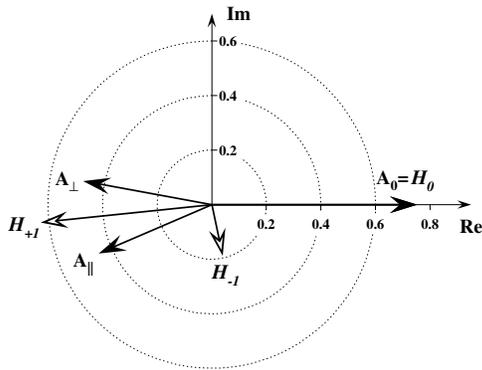
FIG. 16: Representation in the complex plane of the measured transversity amplitudes $(A_0, A_\parallel, A_\perp)$ (Eq. (68)) and the equivalent helicity amplitudes (H_0, H_{-1}, H_{+1}) obtained using Eq. (70). The values for H_+ and H_- are quoted in Table XII.

to the value measured in the charmonium-K^0 modes, $\sin 2\beta = 0.731$ [4], we find

$$\cos 2\beta = +2.72^{+0.50}_{-0.79} \pm 0.27. \qquad (71)$$

The sign of $\cos 2\beta$ is found to be positive at the 86% C.L. This is compatible with the sign inferred from the Standard-Model-based fits of the Cabibbo-Kobayashi-Maskawa triangle, thus limiting the possible presence of unknown physics beyond the Standard Model.

APPENDIX A: UNCERTAINTIES WITH A PSEUDO-LOG-LIKELIHOOD, AND VALIDATIONS

In the angular analysis, the background correction is performed using a pseudo-log-likelihood L', defined in Eq. (26). As L' is not a log-likelihood, the uncertainties yielded by the minimization program (Minuit) [38] that is used are incorrect estimates of the actual uncertainties. The correct estimate is given by

$$\mathbf{Cov}[A] = \mathbf{Cov^H}[A]\left\{ 1 + \left[n_B(1+k)\int b(\boldsymbol{\omega})\left(\frac{\vec{\nabla}g^{b,obs}(\boldsymbol{\omega})}{g^{b,obs}(\boldsymbol{\omega})}\right)^2 \mathrm{d}\boldsymbol{\omega} \right. \right. \qquad (A1)$$
$$\left. \left. + N_B^2 \sigma_k^2 \left(\int b(\boldsymbol{\omega})\frac{\vec{\nabla}g^{b,obs}(\boldsymbol{\omega})}{g^{b,obs}(\boldsymbol{\omega})}\mathrm{d}\boldsymbol{\omega}\right)^2 \right] \mathbf{Cov^H}[A] \right\},$$

where

- $\mathbf{Cov^H}[A]$ is the covariance matrix of A at the maximum of L', estimated by the HESSE routine of Minuit [38] after the fit has converged.

- In the expressions for the bilinear forms $\int b(\boldsymbol{\omega})(\vec{\nabla}g^{b,obs}(\boldsymbol{\omega})/g^{b,obs}(\boldsymbol{\omega}))^2 \mathrm{d}\boldsymbol{\omega}$ and $\left(\int b(\boldsymbol{\omega})\vec{\nabla}g^{b,obs}(\boldsymbol{\omega})/g^{b,obs}(\boldsymbol{\omega})\mathrm{d}\boldsymbol{\omega}\right)^2$, $\vec{\nabla}$ denotes the gradient, i.e., differentiation with respect to the fit parameters A. The "square" is not to be understood as a "scalar product", but as a "direct product", i.e. $\vec{v}^2 = \vec{v}^\dagger \vec{v}$, so that the resulting quantity is a square matrix.

- $g^{b,obs}(\boldsymbol{\omega})$ and $b(\boldsymbol{\omega})$ are the PDFs for the signal and the background. Note that in practice the knowledge of the PDF of the background is not needed for the computation of Eq. (A1) because for any function $h(\boldsymbol{\omega})$, $\int b(\boldsymbol{\omega})h(\boldsymbol{\omega})\mathrm{d}\boldsymbol{\omega}$ is estimated by the average of h over the m_{ES} sideband background

sample:

$$\int b(\boldsymbol{\omega})h(\boldsymbol{\omega})\mathrm{d}\boldsymbol{\omega} \approx \frac{1}{N_B}\sum_{i=1}^{N_B} h(\boldsymbol{\omega}_i). \qquad \text{(A2)}$$

- k is the scaling parameter $k = \tilde{n}_B/N_B$, and σ_k is its uncertainty.

The estimated number of background events in the signal region $\tilde{n}_B$ is obtained from an ARGUS plus Gaussian fit to the m_{ES} spectrum.

The validation of the pseudo-log-likelihood method (i.e., the unbiased nature of the fit parameters, which is not shown here, and of their uncertainties) comes from MC-based studies. We have simulated 10^3 experiments with 10^4 events each [35], using a signal PDF with $\theta_A = \phi_A = \delta_\parallel = \delta_\perp = 1$ rad (as defined in Eq. (5)).

We study the behavior of the fit for various values of the purity, adding the appropriate number of background events. A variety of background shapes have been used. Figure 17 presents results using an ARGUS m_{ES} distribution with an angular distribution of $a + b\cos^2(\theta_{K^*}) + c\cos^4(\theta_{K^*})$ [43].
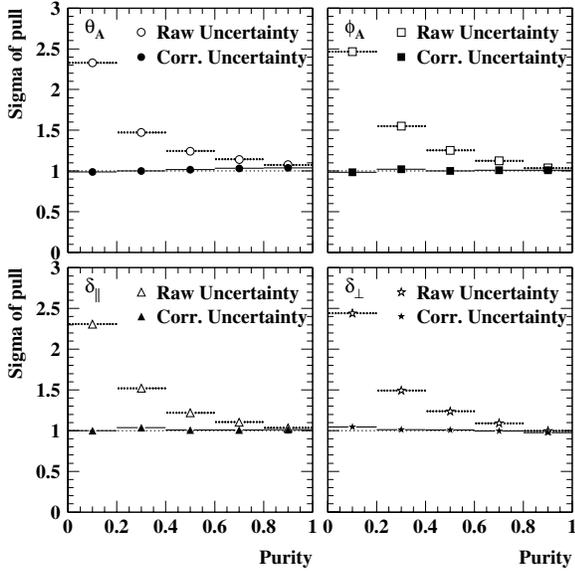

FIG. 17: Root mean square (RMS) of the pull distributions as a function of signal purity (defined in the $5.2 - 5.3$ GeV/c^2 m_{ES} range), for the fitted parameters $\theta_A, \phi_A, \delta_\parallel$, and $\delta_\perp$. Open symbols denote the RMS of the pulls computed with the uncertainties taken directly from Minuit. Closed symbols denote the uncertainties computed according to Eq. A1.

Figure 17 shows the results from the Monte Carlo study. As the purity decreases, the Minuit-reported uncertainties diverge more and more from the actual spread in the results. The uncertainties calculated from Eq. (A1) correctly predict the behavior of the spread, even at low purity.

[1] M. Kobayashi and T. Maskawa, Prog. Theor. Phys. **49**, 652 (1973).
[2] Belle Collaboration, K. Abe *et al.*, Phys. Rev. D **66**, 071102 (2002).
[3] BABAR Collaboration, B. Aubert *et al.*, Phys. Rev. Lett. **89**, 201802 (2002).
[4] Particle Data Group, S. Eidelman *et al.*, Phys. Lett. B **592**, 1 (2004).
[5] M. Gronau and D. London, Phys. Rev. D **55**, 2845 (1997).
[6] B. Kayser and D. London, Phys. Rev. D **61**, 116012 (2000).
[7] R. Fleischer, G. Isidori and J. Matias, JHEP **0305**, 053 (2003).
[8] Y. I. Azimov, Phys. Rev. D **42**, 3705 (1990).
[9] Y. Grossman and H. R. Quinn, Phys. Rev. D **56**, 7259 (1997).
[10] J. Charles, A. Le Yaouanc, L. Oliver, O. Pene and J. C. Raynal, Phys. Lett. B **425**, 375 (1998) [Erratum-ibid. B **433**, 441 (1998)].
[11] T. E. Browder, A. Datta, P. J. O'Donnell and S. Pakvasa, Phys. Rev. D **61**, 054009 (2000).
[12] H. R. Quinn, T. Schietinger, J. P. Silva and A. E. Snyder, Phys. Rev. Lett. **85**, 5284 (2000).
[13] I. Dunietz, R. Fleischer and U. Nierste, Phys. Rev. D **63**, 114015 (2001).
[14] I. Dunietz, H. R. Quinn, A. Snyder, W. Toki and H. J. Lipkin, Phys. Rev. D **43**, 2193 (1991).
[15] J. Charles, A. Le Yaouanc, L. Oliver, O. Pene and J. C. Raynal, Phys. Rev. D **58**, 114021 (1998).
[16] A. S. Dighe, I. Dunietz and R. Fleischer, Eur. Phys. J. C **6**, 647 (1999).
[17] C. W. Chiang, Phys. Rev. D **62**, 014017 (2000).
[18] A. S. Dighe, I. Dunietz and R. Fleischer, Phys. Lett. B **433**, 147 (1998).
[19] BABAR Collaboration, B. Aubert *et al.*, Phys. Rev. Lett. **87**, 241801 (2001).
[20] C. W. Chiang and L. Wolfenstein, Phys. Rev. D **61**, 074031 (2000).
[21] M. Suzuki, Phys. Rev. D **64**, 117503 (2001).
[22] E-135 Collaboration, (LASS), D. Aston *et al.*, Nucl. Phys. B **296**, 493 (1988).
[23] CLEO Collaboration, C. P. Jessop *et al.*, Phys. Rev. Lett. **79**, 4533 (1997).
[24] CDF Collaboration, T. Affolder *et al.*, Phys. Rev. Lett. **85**, 4668 (2000).
[25] Belle Collaboration, K. Abe *et al.*, Phys. Lett. B **538**, 11 (2002).
[26] A. S. Dighe, I. Dunietz, H. J. Lipkin and J. L. Rosner, Phys. Lett. B **369**, 144 (1996)
[27] Stéphane T'Jampens, Thesis (in French), Université Paris XI, 18 Dec. 2002. *BABAR* Thesis-03/016 available at http://www-public.slac.stanford.edu/babar/BaBarPublications.htm.
[28] K. M. Watson, Phys. Rev. **88**, 1163 (1952).
[29] E. P. Wigner, Phys. Rev. 98, 145 (1955).
[30] BABAR Collaboration, B. Aubert *et al.*, Nucl. Instrum. Meth. A **479**, 1 (2002).
[31] G. C. Fox and S. Wolfram, Phys. Rev. Lett. **41**, 1581 (1978).
[32] BABAR Collaboration, B. Aubert *et al.*, Phys. Rev. D **66**, 032003 (2002).
[33] ARGUS Collaboration, H. Albrecht *et al.*, Z. Phys. C **48**, 543 (1990).
[34] Particle Data Group, K. Hagiwara *et al.*, Phys. Rev. D **66**, 010001 (2002).
[35] D. J. Lange, Nucl. Instrum. Meth. A **462**, 152 (2001).
[36] BABAR Computing Group Collaboration, D. H. Wright *et al.*, eConf **C0303241**, TUMT006 (2003) [arXiv:hep-ph/0305240].
[37] GEANT4 Collaboration, S. Agostinelli *et al.*, Nucl. Instrum. Meth. A **506**, 250 (2003).
[38] F. James and M. Roos, Comput. Phys. Commun. **10**, 343 (1975).
[39] W. Dunwoodie, private communication.
[40] Naoki Awaji, Ph.D. Thesis, Nagoya Univ., Nov. 1986.
[41] BABAR Collaboration, B. Aubert *et al.*, Phys. Rev. D **70**, 012007 (2004).
[42] A. Stuart and J. K. Ord, *Kendall's advanced theory of statistics*, Vol. 2, *Classical Inference and Relationship*, 5th Ed.,(Oxford Univ. Press, 1991).
[43] More precisely: $\frac{1}{\sqrt{8\pi}}\mathcal{Y}_{000} + \frac{1}{15}\mathcal{Y}_{040}$.